UNIVERSITAT DE BARCELONA

Final Degree Project

Biomedical Engineernig Degree

Bioprinted gut-on-a-chip to mimic the small intestinal mucosa

Barcelona, June 14 2021

Author: Elena van Breukelen García

Director/s: María García Díaz,

Núria Torras Andrés

Tutor: Elena Martínez Fraiz

Abstract

Organ-on-a-chip (OoC) is an emerging technology which combines microfluidics with cell culture to create platforms that replicate human organs. These predictive models are used to understand human physiology and to predict responses to medical treatments. Being the small intestine the largest interface between the environment and the human organism and one of the most important organs involved in drug metabolism, there is an increasing interest from researchers and the pharmaceutical industry for reliable *in vitro* intestine models. However, currently available gut-on-a-chip devices that replicate the complex microenvironment found in the *in vivo* tissue are scarce, limiting their translational capabilities to clinical outcomes. Therefore, in this work we aim to develop a reproducible gut-on-a-chip device that mimics the 3D architecture and cell heterogeneity of the small intestinal mucosa. SLA 3D bioprinting will be used to fabricate cell-encapsulating GelMA-PEGDA hydrogels that support the formation of an epithelial monolayer on top, to replicate the two compartments of the intestinal mucosa; the lamina propria and the intestinal epithelial barrier. The hydrogels contain fibroblasts and immune cells, which play a key role in maintaining the intestinal mucosa integrity and homeostasis. These scaffolds will be then incorporated into PDMS microfluidic chips to create the final biomimetic system. Although further improvements are needed, this gut-on-a-chip, obtained using precise and fast fabrication techniques, might be a useful tool for drug development and human physiology studies.

Table of contents

1. Introduction

Organ-on-a-chip (OoC) microdevices aim to create *in vitro* models of human organs by simulating the *in vivo* environment found in the tissues, combining microfluidics with cell culture [1]. These predictive models are used to understand the human body functions and the pathogenic mechanisms of disease for drug development and toxicity assessment.

The need for biomimetic systems arises from the major gap between the current *in vivo* and *in vitro* models. In the preclinical phase of drug development, compounds are tested in 2D cell cultures. Although these cultures give primary information on the effect of the substances in cell activity, they are inadequate to predict patient outcomes, as they do not mimic the complex dynamic tissue microenvironment [2]. Therefore, the pharmaceutical industry is interested in the development of platforms that allow for rapid, efficient, cost-saving and reliable drug screening, reducing the need for animal testing [3].

One of the most important organs when studying pharmacokinetics is the gut. Drugs administered through the oral route have to be absorbed in the small intestine in order to enter the bloodstream and be distributed throughout the body. This tissue is formed by several layers, being the intestinal mucosa the innermost layer and in direct contact with the external environment. It is responsible for protection against pathogens, nutrient absorption, and waste secretion, and is made up of an epithelial barrier and an underlying lamina propria, followed by muscular layers [4]. To increase the surface area where nutrients absorb, the tissue presents a characteristic architecture of protrusions, called villi, followed by invaginations, known as crypts [5] (Figure 1). The epithelial monolayer is composed of different cell lineages (enterocytes, enteroendocrines, Paneth cells, Tuft cells, Goblet cells and stem cells) which are characteristically distributed throughout the crypt-villus domains. The most abundant cells are the enterocytes, which are highly polarized absorptive cells that present microvilli on the apical side exposed to shear stress. Differently, the lamina propria is connective tissue with residing fibroblasts, myofibroblasts and immune cells that support the intestine functions and maintain its homeostasis [6].

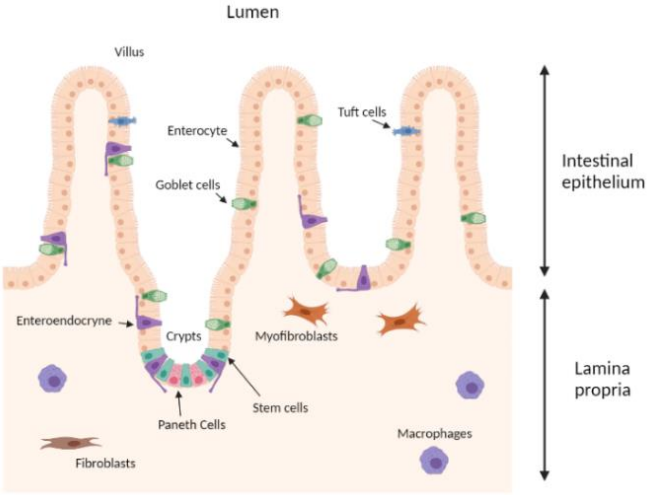

Figure 1. Schematic of the intestinal mucosa with the crypt-villus architecture. The epithelial monolayer is composed of enterocytes, enteroendocrines, Paneth cells, Tuft cells, Goblet cells and stem cells. The underlying lamina propria has residing fibroblasts, myofibroblasts and immune cells that support the intestinal barrier function. (Created in BioRender.com).

Given the complexity of the living tissue, it is challenging to mimic the small intestinal mucosa. Specifically, OoC models that incorporate the structural features and recreate the cell heterogeneity of the gut are scarce. Therefore, this project is focused on fabricating a gut-on-a-chip device, which simulates, on the one hand, the stromal compartment by incorporating a 3D cell-encapsulating hydrogel with crypt-villus architecture and, on the other hand, the intestinal barrier, by growing an epithelial monolayer on top. To create a reproducible and cost-effective system, digital light projection stereolithography (DLP-SLA) 3D bioprinting will be used to fabricate the hydrogels with embedded fibroblasts and immune cells. All of this will be carried out in combination with microfluidic technology to obtain the final gut-on-a-chip device.

1.1. Objectives

The project seeks to fabricate a reproducible gut-on-a-chip device that mimics the small intestinal mucosa. To do so, 3D SLA bioprinting and microfluidic technology will be used in combination with cellular cultures. To meet the primary goal, some secondary objectives are defined:

- To fabricate hydrogel scaffolds using SLA 3D bioprinting.
- To determine the hydrogel scaffold pore size.
- To encapsulate intestinal stromal cells (fibroblasts and immune cells) into the bioprinted hydrogels and assess their behavior in a 3D microenvironment.
- To obtain a model of the intestinal mucosa with epithelial and stromal cells and monitor the barrier properties.
- To obtain a gut-on-a-chip device containing the cell-laden hydrogel and the microfluidic component, and assess cell viability inside the chip.

1.2. Project scope

The project was carried out between the 1st of February and the 22nd of June of 2021 in the Biomimetic Systems for Cell Engineering research group at the Institute for Bioengineering of Catalonia (IBEC). It was divided into different stages, which are explained in detail in *Section 6*. In short, first, a literature review was carried out, followed by an experimental part, and finishing with a result analysis.

For the experimental research, a previous training, completed during the summer months of 2020, was necessary in order to use all the IBEC's facilities and to learn the basic laboratory techniques. The experimental research consisted of the fabrication and characterization of the bioprinted hydrogels, first without cells embedded for pore size determination and then with stromal cells encapsulated. Monocytes and fibroblasts containing hydrogels were fabricated and epithelial cells were seeded on top, mimicking the lamina propria and the epithelial barrier. The co-cultured hydrogels were studied alongside hydrogels laden with immune cells alone, to evaluate their differentiation into macrophages. As it is difficult to incorporate sensors into the microfluidic device, cell behavior inside hydrogels was first studied in static Transwell® models. After verification of epithelial barrier formation and monocyte differentiation in flat hydrogels, the gut-on-a-chip was assembled. This included the microfluidic chip with the cell-laden hydrogel presenting a villus-crypt-like architecture. Owing to the time restrictions, we were not able to develop a fully functional system, thus, further experiments are needed.

1.3. Memory structure

The result analysis was followed by the report preparation and writing. The memory includes a brief introduction containing the motivation and goals of the project. Following, the state of the art of OoC technology and the commercialized products are reviewed. Next, the methodology of the experiments carried out is described and the obtained results are discussed. The report also includes the technical and economic feasibility and viability of the project, as well as the current regulations regarding OoC. Finally, the conclusion and future improvements are stated.

2. Background

2.1. From microfluidics to organ-on-a-chip

OoC based devices appeared over a decade ago as an evolution of Lab-on-a-Chip (LoC), which emerged after the appearance of microfluidic technologies. Microfluidics is the use of microminiaturized devices with different compartments, such as channels, pumps, mixers or separators that support the study of the fluid's behavior. Reducing the scale induces a laminar flow enabling more precise control of the system, all with less sample volume [7]. Therefore, microfluidics has reinforced the development of LoC devices, which integrate multiple laboratory functions for automated cell or molecular analysis into small, compact and portable devices [8].

The OoCs devices can be classified into three different groups: OoCs that emulate the barrier function of a tissue, OoCs that replicate one specific organ, and microfluidic platforms that incorporate multiple interconnected organs to study their interaction [9].

Generally, all OoC devices include two main components, microfluidics and 2D or 3D living cell tissues. The first component comprises the channels that will reproduce the fluid flow in the human body, distributing the nutrients and oxygen throughout the tissue model. Furthermore, the microchannels are used to induce specific states for studying pathological processes or to deliver drugs. For fabrication of the microfluidic chip [10], [11]poly(methyl methacrylate) (PMMA)[12], [13] and polydimethylsiloxane (PDMS) are widely used materials [10], [11],[12], [13]. However, PDMS has become the most popular as it presents unique characteristics including gas permeability, biocompatibility, cytocompatibility elasticity, low cost and optical transparency.

As for fabrication techniques, soft lithography has become the foundation of OoCs fabrication due to its simplicity and low cost. It consists of curing soft elastomers on a master mold with the desired micropatterns. Yet, 3D printing is gaining attention since it allows for automated and high-resolution fabrication while giving the possibility for the direct incorporation of the tissue component into the microfluidic device [14].

The second component in OoC is the cell culture, or biological component, and is simulated with a combination of cells and proteins. Advancements are made on the incorporation of 3D scaffolds that simulate the structural features of the tissue. In this context, hydrogels have drawn most of the attention as these polymeric networks absorb high amounts of water mimicking the extracellular matrix (ECM). Furthermore, their mechanical and chemical properties can be tuned by changing the composition, polymerization method and crosslinking density. For hydrogel fabrication, synthetic (e.g. polyvinyl alcohol, polyethylene glycol, polyacrylic acid, etc.) or natural polymers (e.g. collagen, gelatin, chitosan, alginate, pectin, etc.) can be used [15]. The natural polymers are biocompatible and biodegradable but lack mechanical stability. The synthetic ones provide structural integrity and prevent fast degradation, but they lack cell adhesion motifs. Thus, a combination of the two would give the best results for cell-laden hydrogels with topographical features.

One of the main fabrication techniques of hydrogel scaffolds is bioprinting due to its high resolution, versatility, and throughput. 3D bioprinting can be classified in extrusion-based, inkjet-based, laser-assisted, or stereolithography (SLA) [16]. Among them, SLA presents the best attributes for fabricating cell-encapsulating hydrogels due to its low cost, lack of pressure exertion, and high speed, reducing time exposure of cells to non-physiological conditions [14]. It is based on the projection of UV or white light on the bioink, which consists of a mixture of a photosensitive

prepolymer solution with cells, inducing the photocrosslinking of the biomaterial in a layer-by-layer manner (Figure 2).

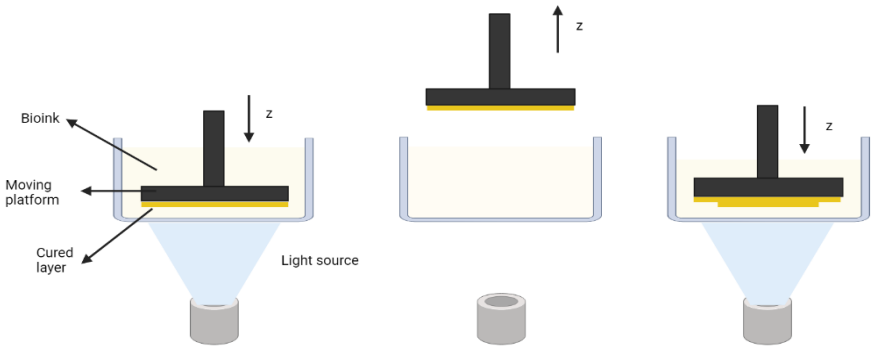

Figure 2. Schematic of working principle of SLA bioprinting technique. A building platform is submerged into the photocrosslinkable prepolymer and light is irradiated triggering the curing of a layer in its surface. Once polymerized the platform moves upwards in the z-direction, after which light is irradiated again with a new pattern, adding a newly cured layer on top of the previous one. (Created in BioRender.com)

2.2. Gut-on-a-chip

Efforts in the gut-on-a-chip field are focused on emulating the absorption and metabolism function of the intestine, incorporating physiological realistic cell types, a 3D villus-crypt architecture, fluid flow and peristaltic motion [17].

The simplest intestine chip models are microfluidic systems with two channels, separated by a porous membrane with immortalized intestinal epithelial cells seeded on top replicating the intestinal barrier [18]. One channel represents the gut lumen whereas the other channel the blood stream, and are both perfused with a continuous laminar flow of culture medium (Figure 3 (a)). These models are mainly used for permeability assays.

The complexity of these systems is increased with the addition of biochemical and biomechanical cues, similar to the one's tissues experience under physiological conditions [9]. The biomechanical cues play a key role in tissue maturation and different gut-on-chip models have been developed to incorporate this increased complexity. On the one hand, it has been proved that the stiffness and topography of the scaffolds can regulate the cell activity and its resemblance to the native human gut [19]. Therefore, villus-shaped structures have been incorporated into the microfluidic device. For example, Shim *et al.* developed a microfluidic gut model that incorporated a 3D villi collagen scaffold fabricated with photolithographic technique (Figure 3 (b)) [20]. On the other hand, mechanical active stimuli such as tensile stretching have been proved to induce epithelial cell polarization and differentiation. Kim *et al.* generated a model with cyclic peristalsis-like mechanical deformations by incorporating two lateral channels subjected to suction cycles (Figure 3 (c)) [10]. The stretching of the channels triggered villus morphogenesis of the epithelial monolayer, which in

static conditions remained flat. Commensal microbes were also integrated into the model, to study their interaction with epithelial cells and their contribution to intestinal homeostasis.

One of the most recent works in this field has been carried out by Lutolf *et al.* [11]. They have developed a hydrogel-based microfluidic chip with a crypt-like architecture that induces organoid morphogenesis (Figure 3 (d)). The 3D topography, obtained with the laser-ablation technique, triggered the differentiation of intestinal stem cells into the distinct cell types found in the intestinal epithelium that were spontaneously arranged across the crypt and villus domains as in the in *vivo* tissue. Moreover, they included stromal cells, such as myofibroblasts and immune cells that supported the tissue barrier function.

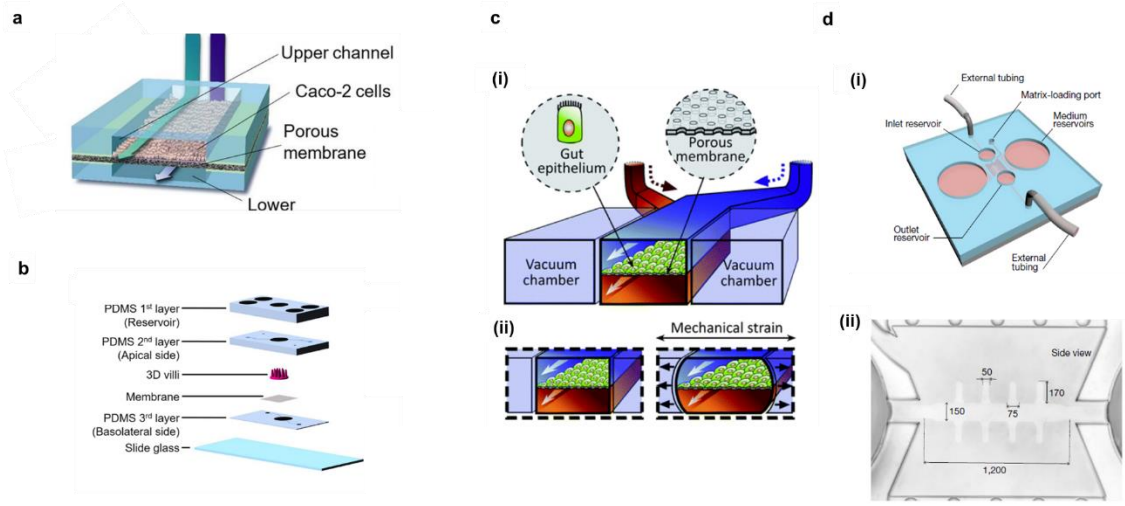

Figure 3. Intestine-on-a-chip devices. (a) Schematic of a simple microfluidic intestinal barrier model, composed of two channels separated by an epithelial monolayer. Adapted from Ref. 18 [18]*(b) Schematic of the assembly of a microfluidic intestinal model with a 3D villus-like collagen scaffold. Adapted from Ref. 20. (c) Schematic of intestine-on-a-chip that recreates the in-vivo mechanical forces. (i) Cross-section of the device with lateral vacuum chambers. (ii) Schematic vacuum chambers suction to generate a cyclic stretch of the membrane. Adapted from Ref 10. (d) Mini-intestine 3D hydrogel-containing microdevice (i) Schematic of the microfluidic device. (ii) Photograph of the top view of the channel with the 3D crypt-shaped hydrogel of collagen/Matrigel and dimensions. Adapted from Ref 11.*

The present study is a continuation of the previous work from the group [21], in which they developed a model of the intestinal mucosa using gelatine methacrylate (GelMA) – poly(ethylene glycol) diacrylate (PEGDA) hydrogel co-networks. This scaffold allowed for the encapsulation of intestinal fibroblasts with high adhesion and viability, as well as the intestinal epithelial monolayer formation on top. A follow-up study encapsulated immune cells together with fibroblasts inside the GelMA-PEGDA hydrogels [22] and demonstrated that this immune component had an important role in the intestinal barrier properties. However, these hydrogels were not incorporated into microfluidic chips and presented no topographical features.

Therefore, we will use the projector-based SLA 3D bioprinting technique to rapidly fabricate well-defined reproducible scaffolds, giving room for automated fabrication. Moreover, we aim to

incorporate an immune component into the stromal compartment to replicate the immune-modulatory functions of the intestine while integrating the hydrogels into a PDMS microfluidic chip. The final complete intestine model is shown in Figure 4.

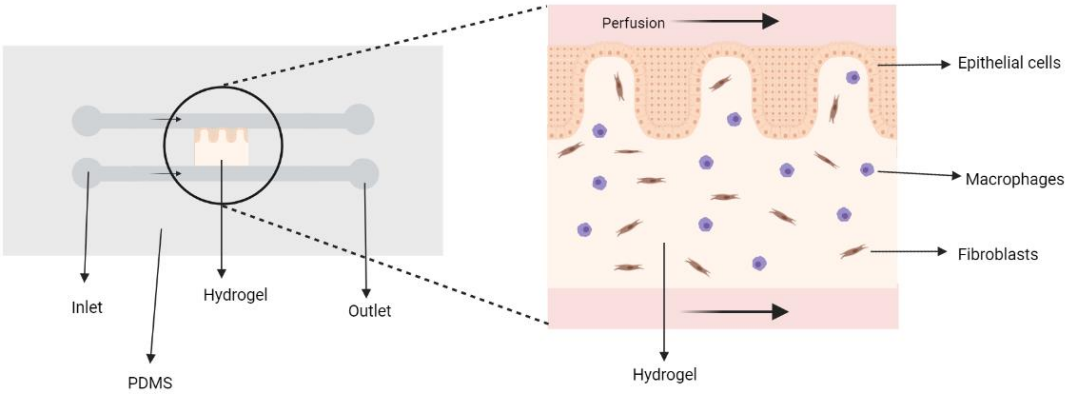

Figure 4. Bioprinted gut-on-a-chip to mimic the small intestinal mucosa. The model is composed of a microfluidic chip with two channels, recreating the lumen and blood-stream, that incorporates a cell-laden hydrogel with crypt-villus architecture and with epithelial cells seeded on top. Created in BioRender.com.

This chip provides several advantages in comparison with already existing models. Firstly, it does not only replicate the epithelial barrier but also the lamina propria and its immune system function. Thus, increasing the complexity and functionality of the model. Secondly, the microfluidic device incorporates an ECM-like matrix with a 3D architecture that resembles the native tissue, combining natural and synthetic polymers. Third, it uses a projector-based SLA bioprinting technique for the fabrication of the constructs. This method allows for high-resolution, mechanically robust and fast cell-laden hydrogel fabrication, that ensures cell viability up to 95% [16], [23]. Lastly, a customized commercially available 3D printer is used, reducing the costs that come from highly specialized bioprinter. Additionally, this printer gives us the possibility of printing several hydrogels simultaneously by increasing the moving platform surface.

3. Market analysis

The OoC concept appeared in 2010 when the first successful lung-on-a-chip device was produced by the Wyss Institute led by Donald Ingber [24]. The same group later founded Emulate, one of the first commercial OoC ventures. They now offer supported models of liver, kidney, and intestine, as well as microfluidic chips that can be configured to emulate many organs. New companies have emerged since, offering different alternatives of single chips; Alveolix, TARA Biosystems, Synvivo or Nortis, to name a few.

TissUse and Hesperos are bringing body-on-a-chip devices to the market with, for instance, the HUMIMC and Heart-liver-skeletal muscle-neuron four organ model, respectively. These models support the study of absorption, distribution, metabolism, and excretion of compounds.

Another pioneer in the field is MIMETAS, who introduced hydrogel-liquid interfaces into their microfluidic chips to mimic the ECM. Furthermore, they also lead the advancements onto creating multi-chip plates for throughput screening (OrganoPlate 2-lane 96). This approach has also been followed by AimBiotech.

Regarding intestine models, Emulate commercializes the Emulate Colon Intestine-Chip that combines organoid-derived epithelium with colon-specific endothelium and mechanical forces. There are no other gut-on-a-chip devices, although we find publications in which research groups use the customizable commercialized models to seed intestinal cells [25].

In 2020 the microfluidic market size was valued at USD 17.9 billion, in which the organ on a chip presence is increasing and is expected to expand at a compound annual growth rate (CAGR) of 21.9%, as it will be adopted by new markets, including hospitals and cosmetic and chemical industries [26].

Given the complexity of the gut, it is challenging to create robust biomimetic microsystems that can be put on the market and so the focus is on integrating the morphological characteristics and dynamic environment while extending the device life span [27]. Furthermore, for improved functional readout, the incorporation of built-in sensors is being studied. Provided that the main end-users are pharmaceutical companies, life science companies, research institutes and contract research organizations, who are looking for efficient and cost-saving techniques for *in vitro* testing, the industry is questing to find a balance between complexity and costs. The final goal is to create reproducible, simple, and cost-effective systems for commercial use. Therefore, this project aims at creating a gut-on-a-chip that satisfies the current demands of the market using 3D bioprinting.

The use of 3D bioprinting technology to fabricate hydrogel scaffolds that can be integrated in the microfluidic chip has not been adopted yet by the developers. The bioprinting concept appeared in the early 2000s when its potential for tissue engineering, therapeutic or drug screening applications was discovered. Organovo is considered the first 3D bioprinting company, specialized in fabricating tissue models with inkjet-based modality, and was followed by RegenHu and Poietis in the commercialization of extrusion-based and light-based 3D bioprinters, respectively. However, owing to the high costs, research groups opted for the adaption of commercially available 3D printers to create tissue constructs. Consequently, Allevi, CELLINK and Se3D emerged with affordable general bioprinters [28]. The market was valued in 2020 at USD 1.4 billion and is expected to grow due to the increasing research in organ bioprinting for transplantation [29].

4. Concept engineering

4.1. Cell culture

The intestine has a complex microenvironment, formed by different cell types that support its function. Enterocytes, which are hyperpolarized epithelial cells, are the most important constituents of the intestinal barrier. Although this epithelial barrier plays a key role in protection against pathogens and nutrient absorption, many other cell types found in the underlying lamina propria are crucial for supporting this barrier function while maintaining homeostasis [4]. To name a few, macrophages, lymphocytes, fibroblast, and myofibroblasts. For the fabrication of a 3D model of the gut, three different cell cultures were used: NIH-3T3 as fibroblasts, THP-1 as monocytes that are differentiated into macrophages, and Caco-2 BBe as enterocytes.

4.1.1. NIH-3T3 fibroblasts

The NIH-3T3 (ATCC® CRL-1658™) is a mouse embryonic fibroblast cell line. The cells are cultured in flasks with Dulbecco's Modified Eagle's Medium (DMEM Medium) (Gibco) supplemented with 10% (v/v) of Fetal Bovine Serum (FBS) (Gibco) and 1% of (v/v) Penicillin/Streptomycin (Pen/Strep) (Sigma-Aldrich). We will refer to this medium as Supplemented DMEM. They are incubated at 37ºC and 5% CO_2. Cells were subcultured when reaching 80-90% confluency. To do so, the culture medium from the flask was discarded, and cells were washed with phosphate-buffered saline solution (PBS) (Thermo Fisher) to eliminate all the remains of serum containing trypsin inhibitors. Afterwards, cells were incubated with Trypsin-EDTA (Thermo Fisher) solution for 5 min, or until they were detached from the surface. Supplemented DMEM was added to inhibit trypsin enzymatic activity and cells were centrifuged at 1200 rpm for 5 min. The pellet was then resuspended and seeded in a new flask at a ratio of 1:10.

4.1.2. Brush border expressing human epithelial colorectal adenocarcinoma (Caco-2 BBe)

The Caco-2 BBe cells (ATCC® CRL-2102™) are cloned from the human colorectal adenocarcinoma derived cell line, Caco-2. The cells form a polarized monolayer with an apical brush border (BB). They are cultured in flasks with Supplemented DMEM at 37ºC and 5% CO_2. Cells were subcultured when reaching 80-90% confluency. As explained above, cells were washed with PBS and trypsinized. After blocking the trypsin activity with Supplemented DMEM, cells were centrifuged at 900 rpm for 5 min. The pellet was then resuspended, and the 250.000 cells were seeded in a new T75 flask.

4.1.3. THP-1 monocytes

The THP-1 (ATCC® TIB-202™) is a human leukemia monocytic cell line. The cells are cultured with Roswell Park Memorial Institute (RPMI)-1640 medium (Gibco) supplemented with 10% (v/v) FBS, 1% (v/v) P/S, 1% (v/v) sodium pyruvate (Gibco), 1% (v/v) 4-(2-hydroxyethyl)-1-

piperazineethanesulfonic acid (HEPES) (Gibco) and 0.1% (v/v) β-mercaptoethanol (Gibco), which was added just before use. We will refer to this medium as Supplemented RPMI. They are cultured in suspension at a density of $2x10^5$ cells/mL in non-adherent T75 culture flasks and incubated at 37ºC and 5% CO_2. When cell concentration arrived at a maximum of $1x10^6$ cells/mL they were subcultured by dilution with Supplemented RPMI to reach a concentration of $2x10^5$ cells/mL.

In some experiments, THP-1 cells were differentiated into macrophages-like cells (M0). To induce the differentiation, $8x10^6$ cells were seeded in a petri dish with Supplemented RPMI with phorbol 12-myristate 13-acetate (PMA) at 50 ng/mL. After 72 h, the medium containing PMA was discarded, cells were rinsed with PBS and incubated with 3mL Accutase® cell detachment solution for 10 min in the incubator. With the help of a cell scraper, cells were carefully detached from the surface and 7 mL of Supplemented RPMI Medium was added to inactivate the Accutase® enzymatic activity. Lastly, the suspension of differentiated THP-1 was centrifuged at 400xg for 5 min with a slow deacceleration.

4.2. Synthesis of gelatin methacryloyl (GelMA)

Gelatin methacryloyl (GelMA) is synthesized by the reaction of gelatine with methacrylic anhydride (MA) following the method described previously [30]. The methacryloyl groups of MA react and bond to the amino groups present in the side chains of gelatin, forming modified gelatin that can be photocrosslinked.

Gelatin from porcine skin type A (Sigma-Aldrich) was dissolved in sterile PBS at a concentration of 10% (w/v) at 50ºC for 1 h. Then, the MA (Sigma-Aldrich) was added to the gelatin solution at 0.5 mL/min using a syringe pump (NE-1000 Programmable Single Syringe Pump, New Era) to get a final concentration of 1.25% (v/v) MA. After complete addition, the reaction was kept under stirring conditions at 50ºC for 1 h. The solution was then centrifuged at 1200 rpm for 3 min at 20ºC to remove the unreacted MA. The supernatant was diluted in warm PBS (40ºC) to double its volume to stop the reaction. Finally, the solution was dialyzed against MiliQ water bath at 40ºC using dialysis membranes (Spectra/Por® 1 Dialysis Membranes, MWCO 6000 to 8000, Spectrum ®), previously hydrated. This step is required to eliminate all the byproducts and unreacted MA. The membranes were left for 3 days in MiliQ water, which was changed three times a day. Finally, the pH of the GelMA solution was adjusted at 7.4, distributed in 50 mL falcon tubes and lyophilized for 3-4 days to obtain a foamy solid. The final product is then kept in the freezer at -20ºC until use.

4.2.1. Determination of the degree of functionalization of GelMA

The degree of methacrylation of the GelMA used in the bioink will affect the fabrication conditions and the properties of the hydrogel [30]. This property is quantified by the TNBSA assay, a method developed by Habeeb 1966 [31]. When MA reacts with gelatin, it bonds to reactive amine groups found in the lysine residues, decreasing their availability. Trinitrobenzene sulfonic acid (TNBSA)

reacts with the still available amino groups in an aqueous solution at pH 8 and produces an orange-colored derivative, whose absorbance at 335 nm can be measured. Therefore, by measuring the absorbance, the number of free amino groups can be quantified, and thus the methacrylation.

To perform this assay gelatin and GelMA (known and unknown concentration) were dissolved in carbonate buffer (0.1 M NaHCO3, pH 8.4) (Sigma-Aldrich) at a concentration of 2 mg/mL. To generate a standard curve, a serial dilution of 100 µL of gelatin and GelMA solutions were placed in a 96-well plate (Thermo Scientific™). Wells with only carbonate buffer were also added as blank. Then, 50 µL of working solution (TNSBA 0.01% in carbonate buffer) (Sigma-Aldrich) was added and the plate was incubated at 37ºC for 2 h in the dark. Next, the reaction was stopped and stabilized by adding 50 µL of sodium dodecyl sulfate (SDS) (Sigma-Aldrich) at 10 % (w/v) and 25 µL of HCl 1 M in Milli-Q water to each well. Absorbance was measured at a wavelength of 335 nm with a microplate reader (Infinite M200 PRO Multimode Microplate Reader, Tecan). The resulting values were used for calculating the degree of methacrylation of GelMA, comparing the calibration curve of the gelatin solution (total of free amines available) to the calibration curve of the GelMA solution.

Finally, the percentage of methacrylated lysines, also known as the degree of methacrylation, was calculated with Equation 1.

$$Degree\ Methacrylation = 100 - \%\ free\ amines \qquad Eq.\ 1$$

4.3. Hydrogel fabrication

4.3.1. Bioink preparation

The fabricated hydrogels should have robust mechanical properties that allow for the printing of the hydrogel channel with villus-like microstructures as well as cell adhesion motifs that allow for cell encapsulation, proliferation, and migration. For this reason, the polymer solution (bioink G8) is composed of 5% (w/v) GelMA, suitable for cell adhesion and biodegradable, 3% (w/v) poly(ethylene glycol) diacrylate (PEGDA) (Sigma-Aldrich), synthetic polymer that provides mechanical stability, (0.4% w/v) lithium phenyl-2,4,6-trimethylbenzoylphosphinate (LAP) (TCI Chemicals) as photoinitiator and (0.025% w/v) tartrazine (Sigma-Aldrich) as photo absorber. This last component is a synthetic dye that acts as a photo blocker by absorbing light at 405 nm and is crucial for enabling high print resolution.

To prepare the G8 bioink, PEGDA, LAP and tartrazine were dissolved in Hank's Balanced Salt Solution (HBSS) (Gibco) supplemented with 1% (v/v) Pen/Strep at 65ºC for 1 h and then filtered using a 0.22 µm filter. In parallel, GelMA was dissolved in supplemented HBSS at 65ºC. Once completely dissolved, equal volumes of the two polymer solutions were mixed to obtain the G8

bioink. For cell encapsulation, NIH-3T3 and/or THP-1 were trypsinized as explained above and counted to have a concentration of $6.5x10^6$ cells/mL each. The desired volume of cell suspension was extracted and centrifuged. After centrifugation, the supernatant is carefully removed and directly resuspended in the polymer solution, to obtain the cell-containing G8 bioink.

4.3.2. Substrate silanization

The silanization with vinyl groups of the substrate on which the hydrogel is fabricated, round coverglass (VWR, 13 mm diameter) or polyethylene terephthalate (PET) membranes (it4ip, 10 mm diameter, 0.4 µm pore size), improves its attachment upon printing. In this process, the surface of the substrate is activated with a UV ozone cleaner (ProCleaner™, Bioforce Nanosciences) for 15 min. Directly after, the substrates were incubated in a solution containing 2% (v/v) 3-(trimethoxysilyl)propyl methacrylate (Sigma-Aldrich), 3% (v/v) acetic acid (diluted 1:10) and 95 % (v/v) absolute ethanol for 2 h and then rinsed thoroughly with ethanol. Then, the substrates were placed in the oven at 65ºC for 30 min. Silanized substrates were stored in the vacuum desiccator until use.

4.3.3. 3D bioprinting of the hydrogel

The hydrogels were fabricated using SLA bioprinting. The printing setup was a customization of the commercially available Solus 3D printer (Junction3d), a DLP (digital light processing) projector-based SLA printer (Figure 5). The printing setup consists of a vat, adapted to the small dimensions of the hydrogels, pre-heated at 37ºC where the bioink is introduced. The light is projected through an HD beam projector coupled to an infrared cut-off filter to restrict the light projection to the visible range. Additionally, the printer has a building platform attached to a z-axis actuator where the substrate (silanized PET or coverglass) is attached and the hydrogel will be printed.

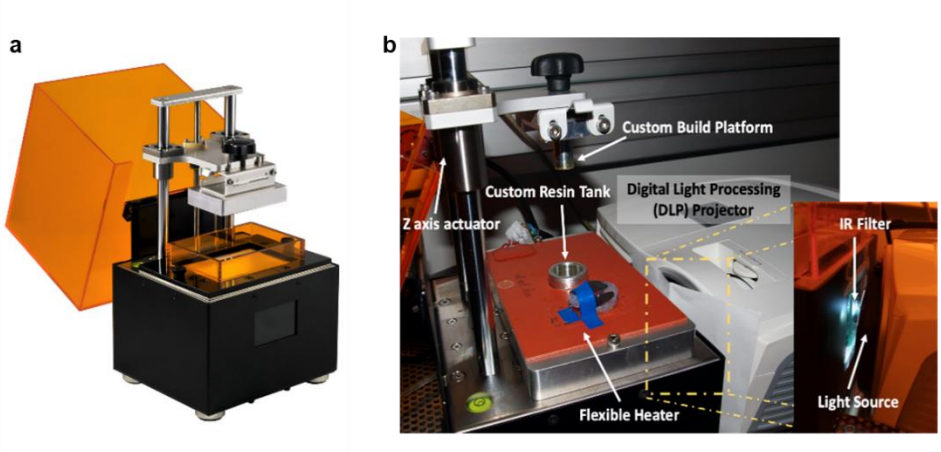

Figure 5. (a) Commercially available Solus 3D printer (Junction3d). (b) Customized Solus 3d printer set up, with miniaturized tank and build platform for hydrogel printing.

The printing process entails different steps. First, a 3D CAD design with the desired structure is created with the modeling software program FreeCAD. Two different designs were employed for different purposes. On the one hand, hydrogel discs of 6.5mm in diameter and 300µm in height

were printed for the preliminary static measurements in Transwell® inserts (Figure 6 (a)). This simple design is used for studying the behavior of cells when being embedded in polymeric scaffolds. On the other hand, rectangular hydrogels (7x4x0.5mm) with micropillars that resemble the 3D villi intestinal architecture were fabricated for gut-on-a-chip experiments (Figure 6 (b)).

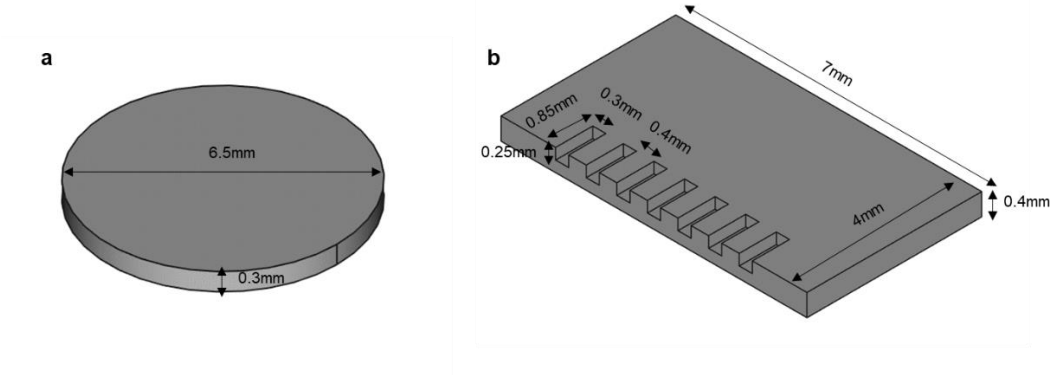

Figure 6. Hydrogel FreeCAD designs. (a) Disc design for static measurements in Transwell® inserts. (b) Rectangular channel-like design with micropillars.

The design is uploaded to the printer software and the proper printing parameters, regarding build resolution and layer printing parameters, are chosen. Then the printing process goes as follows: the liquid polymer solution is introduced into the tank. The building platform is submerged in the mixture and its surface is then irradiated with a light pattern, triggering the photopolymerization of a thin layer. Once the solution has polymerized the building platform moves upwards in the z-direction and light is irradiated again with a new pattern, adding a newly cured layer on top of the previous one. This process continues layer-by-layer until obtaining a 3D structure with the desired morphology. After printing the hydrogels were rinsed with warm PBS and removed from the platform.

Moreover, the printing parameters used for fabricating the hydrogels were optimized to have the appropriate mechanical properties, whilst ensuring cell viability. The optimized values are hereunder detailed:

- Layer thickness: 13μm
- Layer exposure time: 5s
- Initial layer exposure time: 15s
- Number of initial layers: 2
- Exposure buffer time: 1s

4.3.4. *Transwell assembly*

For cell experiments, hydrogels fabricated onto PET membrane substrates were mounted on modified Transwell® inserts as described in [21], [32] (Figure 7). Briefly, the standard polycarbonate membrane was removed from the inserts. Then, a first ring of pressure-sensitive adhesive (PSA) with a 6.5 mm inner diameter and 13 mm outer diameter was attached to the Transwell® insert.

The hydrogel-containing membrane was then adhered to the PSA ring. Finally, a second PSA ring was attached to the bottom of the PET to prevent leakage. Afterwards, 200 μL of PBS (or Supplemented DMEM when encapsulating cells) were added to the upper compartment and 600 μL to the lower compartment.

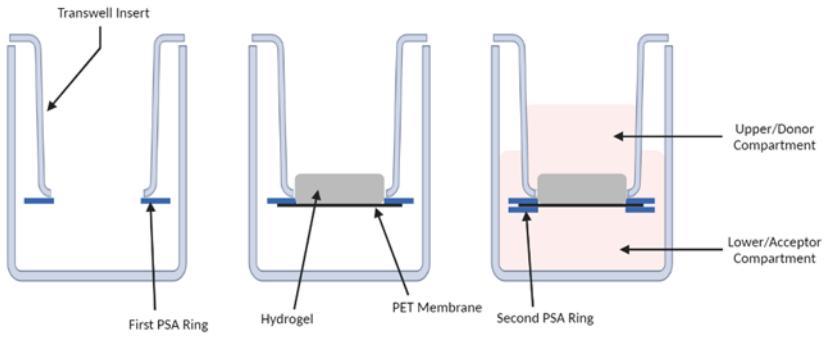

Figure 7. Schematic of the Transwell® assembly process. Created with BioRender.com.

4.4. Characterization of hydrogel network

The structural characterization of the hydrogels is of great interest as it affects cell behavior [33]. Besides, our hydrogels encapsulate intestinal stromal cells such as monocyte-derived macrophages. Thus, we are interested in knowing whether the PMA molecule, which induces the differentiation of THP-1 towards macrophages, can diffuse through the hydrogel.

To determine the pore size of the hydrogels, we measure the permeation of dextrans with a defined size. Thus, fluorescently-labeled dextrans (Merck Life Science) of different molecular weights were used: 4 kDa, 70 kDa, 150 kDa, 500 kDa and 2000 kDa. Hydrogels were printed on silanized PET membranes and mounted on Transwell® inserts and kept in PBS. As controls, PET membranes without hydrogels were mounted on Transwells®. The following day, hydrogels were equilibrated at 37ºC in the incubator. Warmed dextran solutions of a concentration of 0.5 mg/mL in PBS were placed to the upper (donor) compartment and samples of 50 μL were taken from the lower (acceptor) compartment at different time points during 4 h and transferred to a 96 well black plate. The fluorescence of the plate was measured with a Multimode Microplate Reader (Infinite M200 PRO Multimode Microplate Reader, Tecan). Depending on the fluorescent label, FITC or Rhodamine B, the fluorescence was measured at the following excitation and emission wavelengths:

a. FITC: λ_{exc} = 490 (+/- 10) nm; λ_{em}= 525 (+/- 20) nm
b. Rhodamine B: λ_{exc} = 540 (+/- 10) nm; λ_{em}= 625 (+/- 20) nm

From the intensity, the permeated amount of the different dextrans along time was determined. To do so, the fluorescence values are interpolated in the calibration curves to obtain the concentration

of dextran at the different time points. Using Equation 2 we can then calculate the total mass transfer at each time point, a measure of the hydrogel's permeability.

$$Total\ mass\ transfer = V_s * \left(\sum_{n=1}^{n} C_{n-1}\right) + C_n * V_r \qquad Eq.\ 2$$

The values of the mass transferred are then plotted as a function of time to discard those samples that present leakage. Namely, those whose tendency line does not go through the origin. The diffusion coefficient in the hydrogels of each dextran was also calculated using the equations from Engberg *et al*. [34]. (see Appendix A).

4.5. Cell-laden hydrogels mimicking the intestinal mucosa

Hydrogels encapsulating NIH-3T3 and/or THP-1 cells were bioprinted as explained above. These cell-encapsulating scaffolds were then assembled in Transwell® inserts and kept in culture with Supplemented DMEM medium containing Normocin (Invitrogen) (dilution 1:500) so that contamination is prevented. To mimic the intestinal epithelial barrier, Caco-2 BBe cells were seeded on top of the hydrogels at a density of 250.000 cells/sample either at day 1 or day 6 after hydrogel fabrication, and cultured for 21 days, changing the media every other day and monitoring the transepithelial electrical resistance (TEER) throughout the culture.

4.5.1. Transepithelial electrical resistance (TEER)

The transepithelial electrical resistance is a parameter essential for measuring the integrity of the cell monolayer. The TEER is measured through two electrodes, situated one at each side of the cellular barrier, that generate a voltage difference, provoking current to flow. With the current values and ohm's law, the resistance of the samples can be obtained and normalized to the area of the monolayer.

For TEER measurements the EndOhm-6G Chamber and the EVOM3 (Epithelial Voltohmeter) meter from World Precision Instruments were used. The EndOhm chamber is a glass cylindrical chamber with a circular electrode on the bottom and the opposing top electrode on the cap. To avoid TEER changes caused by temperature fluctuations, samples were equilibrated at room temperature for 15-20 minutes. Then, the Transwells® were inserted in the EndOhm chamber and the resistance value was obtained.

The blank value, the resistance of the hydrogel without Caco-2 BBe, was subtracted from the acquired resistance values after seeding to get the resistance derived only from the epithelial monolayer (R_{cell}). Then, the data was normalized to the surface of the hydrogel ($A_{hydrogel}$) following Equation 3. The $A_{Hydrogel}$ of our samples was 0.33 cm^2.

$$TEER = R_{Cell} * A_{Hydrogel} \qquad Eq.\ 3$$

4.5.2. *PMA-induced differentiation of THP-1 monocytes into M0 macrophages inside the hydrogels*

To mimic the intestinal mucosa with immunocompetent features, we encapsulated THP-1 cells inside the hydrogels and co-cultured with NIH-3T3 and Caco-2 BBe epithelial cells. In order to study whether it is possible to differentiate the encapsulated THP-1 cells into macrophages with PMA and the effect of this molecule on the epithelial monolayer, different conditions were tested. On day 18 after printing, PMA at 81 nM (50 ng/mL) [22] or 200 nM [35] was added in the culture media for inducing cell differentiation, only in the apical compartment or in both apical and basolateral compartments. Samples without the addition of PMA were kept as controls. The effect of the PMA on the intestinal epithelial monolayer was evaluated with the TEER. Finally, the analysis of the macrophage cell differentiation was performed by flow cytometry explained in the following section (*Section 4.6*) .

In a parallel experiment and in order to study the macrophage differentiation without the effect of other intestinal cells, either THP-1 or differentiated M0 cells were encapsulated alone into hydrogels. Then, three differentiation conditions were studied: non-differentiated THP-1 hydrogels, M0 hydrogels and THP-1 hydrogels treated with 200 nM PMA for 3 days. Afterwards, cells were recovered from the hydrogels and the degree of differentiation was analyzed by fluorescence-activated cell sorting (FACS).

4.6. Evaluation of the degree of THP-1 differentiation into M0 macrophages inside the hydrogels

4.6.1. *Hydrogel degradation with Collagenase type II*

In order to recover the encapsulated cells, the hydrogels were digested with collagenase as described in [35]. To optimize the conditions and assess the cell viability after the recovery, scaffolds encapsulating NIH-3T3 were used. To achieve this, hydrogel discs were printed encapsulating NIH-3T3 at a density of $7.5x10^6$ cells/mL. The hydrogels were mounted on Transwell® inserts and kept in culture with supplemented DMEM medium. The hydrogels were digested at different time points: the same day of printing, one week after printing, and two weeks after printing, and viability was checked by cell counting and seeding. Once the process was optimized, hydrogels mimicking the intestinal mucosa were used for hydrogel digestion and further FACS analysis.

For samples containing the epithelial cell monolayer, a previous step before the hydrogel digestion is required. The epithelial cell monolayer was first detached incubating the hydrogels with Accutase

for 10 min at 37ºC. The cell suspension was then recovered, neutralized with supplemented media and saved for later to be centrifuged together with the recovered cells from the hydrogels. Hydrogel digestion was achieved using collagenase type II. This enzyme was diluted at a concentration of 300 U/mL in warm filtered PBS. The hydrogels were then removed from the Transwell® inserts, rinsed in PBS and transferred to an Eppendorf tube with 2 mL of filtered collagenase solution. For FACS analysis, 3 hydrogels were pooled and digested per sample. The Eppendorfs were left in the incubator at 37º for 45 minutes, or until the hydrogels were completely dissolved, mixing vigorously with the pipette every 10 min. Then, the PET membranes were removed, and samples were centrifuged at 300xg for 5 min. The cell pellet was resuspended in 100 μL of supplemented DMEM medium for cell viability studies, or FACS buffer for immunophenotyping analysis as explained in the following section.

4.6.2. Flow cytometry direct immunophenotyping

To assess the differentiation state of the immune cells, a direct immunophenotyping and flow cytometry analysis was performed. We used CD11b Antibody (Thermo Fisher) as membrane marker specific for the differentiated THP-1 (M0), the CD31 (PECAM-1) monoclonal antibody (Thermo Fisher) as extracellular marker specific for both differentiated and non-differentiated monocyte, and DAPI for cell viability. An isotype control is required to determine the non-specific binding of the marker. After hydrogel digestion and cell recovery, the pellet was resuspended in 100 μL of ice-cold FACS Buffer; 10% (v/v) FBS and 1% (w/v) sodium azide (Sigma Aldrich) in PBS. Then 5 μL of the desired antibodies was added, and the samples were incubated at 4ºC in the dark for 30 mins. Cells were then centrifuged and washed twice with 500 μL FACS buffer. Finally, the samples were resuspended in 250 μL of FACS buffer and filtered with 70 μm cell strainer before being analyzed with the flow cytometer (Gallios Research Flow cytometry, Beckman Coulter).

4.7. Gut-on-a-chip assembly

After cell-laden hydrogel characterization, scaffolds with the 3D villi channel structure encapsulating THP-1 and NIH-3T3 were printed onto a coverglass and assembled into a PDMS microfluidic chip. The chip is formed by two patterned sheets of PDMS, cured into a 3D printed mold. The bottom PDMS layer contains a small cavity in which the coverglass perfectly fits. The top PDMS layer contains the cavity in which the hydrogel is embedded and the channel features. Two different chip designs were used: single-channel (Figure 8 (a)) and two-channel chip (Figure 8 (b)). To seal the chip and prevent leakage between the PDMS layer, a chip holder was designed, consisting of a 3D printed case with screws (Figure 8 (c)). In Figure 8 (d) a schematic of the PDMS microfluidic chips with the custom-made chip holder is shown. Once the whole gut-on-a-chip was assembled, it was perfused with supplemented DMEM medium at a constant flow rate of 2.5 μl/min using a syringe pump (NE-1000 Programmable Single Syringe Pump, New Era) and left in the incubator at 37ºC and 5% CO_2 (Figure 8 (e)).

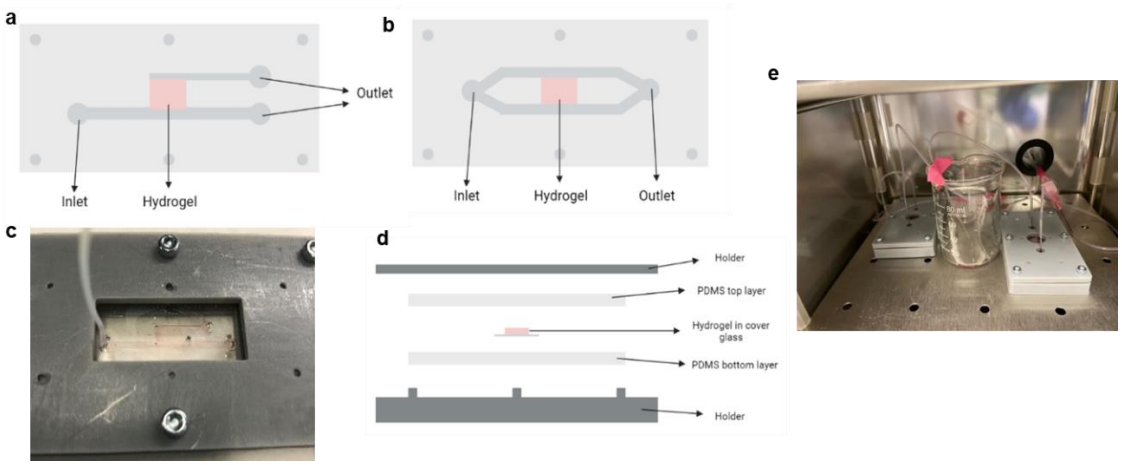

Figure 8. Microfluidic chip and custom-made chip holder. (a) Single-channel chip illustration. (b) Two-channel chip illustration. (c) Single-channel chip and holder system with perfused medium. (d) Chip and holder assembly schematics. (e) Chip perfusion set up.

4.7.1. Cell viability assay

The viability of the encapsulated cells inside the hydrogels on the chip was assessed using the Live/Dead™ viability/cytotoxicity assay kit (Invitrogen). After 5 or 7 days, the chips were disassembled and hydrogels were washed three times with warm PBS and incubated for 20 min with 4μM ethidium homodimer-1 (EthD-1), 2μM calcein AM and Hoechst (dilution 1:1000) in PBS at 37 ºC. Afterward, the samples were washed and analyzed with the confocal microscope (LSM 800, Zeiss). EthD-1 will only stain the nuclei of dead cells in red, whereas the non-fluorescent calcein AM will be converted into fluorescent calcein only by living cells. Then, cell viability quantification was performed manually stack by stack.

5. Detail engineering

5.1. Determination of the degree of functionalization of GelMA

Through the methacrylation process, gelatin becomes a photocrosslinkable and thermostable polymer, which can be used in photopolymerization printing of hydrogels. The degree of methacrylation determines the mechanical properties of the GelMA as well. Thus, by varying the ratios of gelatin to MA in GelMA synthesis the stiffness of the scaffold can be tuned. Studies suggest that the appropriate degree of methacrylation ranges between 30% and 60% [36]. Lower values lead to low crosslinking and hydrogels with no structural integrity, whereas high values result in hard scaffolds that reduce cellular spreading and proliferation [37].

We performed the TNBSA assay to determine the extent of substitution of free amine groups in newly methacrylized GelMA (B6), which is expected to be around 40% for a MA concentration of 1.25% (v/v) and compare it with the previous GelMA batch (B5). The batch B5 and new batch B6 had 44% ± 6 and 34% ± 2 occupied amine groups, respectively. These percentage values were a

bit lower than expected, yet they were still in the suitable range for hydrogel fabrication and subsequent cell adhesion.

5.2. Characterization of hydrogel network

Hydrogels are crosslinked polymeric networks and thus present a pore architecture. The mesh size determines cell attachment, survival, migration, and proliferation, as well as ECM secretion [38]. Research shows that small pore size increases initial cell attachment, but that larger pore improves infiltration and so long-term viability [33]. Besides, porosity is correlated to swelling, stiffness and molecular diffusion of nutrients to and metabolites out of the scaffold. In our work, the determination of the hydrogel pore size is crucial to know if the PMA molecule would diffuse through the hydrogel. The PMA molecule activates THP-1 cells which differentiate into macrophages. These phagocytic cells play a major role in maintaining intestinal homeostasis. Although differentiated macrophages can be directly embedded in the hydrogel [22], encapsulation of the monocytes is preferred, as the fabrication process may affect cell phenotype. To differentiate them inside the scaffolds, the PMA molecule should diffuse through the hydrogel.

The hydrogel pore size can be estimated using the diffusion of dextrans of different molecular weight (Figure 9).

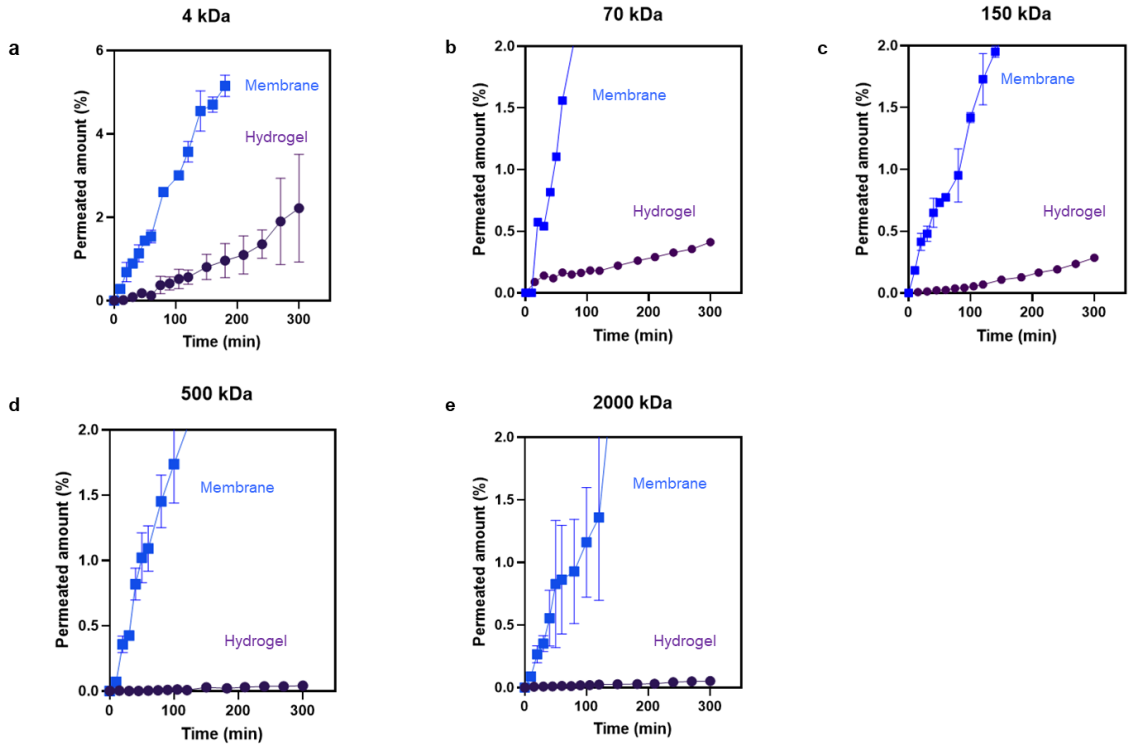

Figure 9. Amount of permeated dextran through the hydrogel on top of a PET membrane, and the PET membrane alone, as a function of time. (a) 4 kDa dextran with a 1.4 nm radius. (b) 70 kDa dextran with a 5.8 nm radius. (c) 150 kDa dextran with an 8.5nm radius. (d) 500 kDa dextran with a 16 nm radius. (e) 2000 kDa dextran with a 20.8 nm radius. The values shown are mean ± SD, n>2.

The FD4 dextran, which has a radius of 1.4 nm, passed freely through the hydrogel. The FD70 and FD150 were also able to permeate, although the hydrogel hampered their movement. Finally, the permeated amount of FD500 and FD2000 was below the limit of detection, meaning that they were not able to diffuse through the hydrogels. Considering the results, we can estimate that the average pore size is between the radius of the 150 kDa and 500 kDa dextran, meaning between 8.5 nm and 16 nm and larger molecules will be not able to permeate through the mesh. Having a molecular weight of 616.8 Da and a radius of 1.1 nm, the PMA molecule will easily diffuse through the hydrogel reaching the encapsulated THP-1 cells. Other small molecules important to ensure cell viability, such as oxygen and glucose, are also able to diffuse.

5.3. Characterization of cell-laden hydrogels mimicking the intestinal mucosa

The 3D model of the intestinal mucosa was bioprinted using the G8 bioink. The model contained encapsulated NIH-3T3 fibroblasts and THP-1 cells as stromal compartment and Caco-2 BBe enterocytes forming the epithelial barrier. In order to better characterize the cell behavior, hydrogels were first studied in static conditions assembled into Transwells® (Figure 10 (a)). Thus, standard cell culture assays such as the evaluation of the epithelial monolayer's integrity through TEER measurements can be performed.

In previous works using a similar intestinal mucosa model, epithelial cells were seeded on top of the hydrogel one day after fabrication [21]. However, it was observed that during the first week after seeding, the epithelial barrier was not yet formed, and the TEER values did not increase. This lag phase was probably due to the lack of secreted ECM from the stromal compartment. Thus, we first studied the epithelial monolayer formation on top of cell-laden hydrogels seeded 1 or 6 days after hydrogel fabrication. The TEER was monitored throughout the culture (Figure 10 (b)). From the beginning of the culture, samples seeded one week after fabrication showed TEER values higher than the samples following the standard procedure (seeded 1 day after fabrication), reaching the TEER plateau after 2 weeks of culture instead of the 3 weeks needed for the cells seeded at day 1.

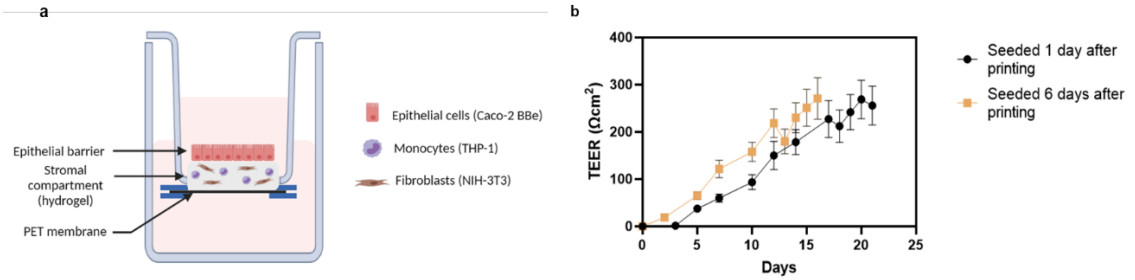

Figure 10. (a) 3D model of the intestinal mucosa in Transwell® inserts, composed of hydrogel with embedded NIH-3T3 and THP-1 and a monolayer of Caco-2BBe. (b) TEER values for different seeding times, 1 day after printing and 6 days after printing, as a function of seeding days. The values shown are the Mean ± SEM, n>9.

With these results, we can conclude that the interaction and cross-talk between epithelial and stromal cells enhance the growth and formation of the epithelial barrier. Fibroblasts need time to adhere to the hydrogel and secrete ECM. If we allow the cells to migrate and proliferate before seeding, we can reduce the amount of time that enterocyte cells require to establish tight junctions and form a selective permeable epithelial barrier.

5.4. PMA induced differentiation of THP-1 monocytes into M0 macrophages inside the hydrogels

Intestinal macrophages are mononuclear phagocytes primarily found in the lamina propria, responsible for maintaining mucosal homeostasis and intestinal barrier integrity. Overall, they are accountable for the intestinal immune response [39]. Thus, if incorporating these cells into our bioprinted intestinal mucosa we would obtain a model with increased functionality and immune-competent features. Macrophages can be incorporated into the hydrogel already differentiated [22] or as monocytes that can be later differentiated into macrophage-like cells [35]. To do this, we first need to evaluate the differentiation of monocytes inside the hydrogel, without disrupting the epithelial monolayer.

5.4.1. Effect of PMA on epithelial monolayer integrity.

Co-cultured hydrogels were exposed to different concentrations of PMA (81 and 200 nM) and the effect on the epithelial integrity was monitored. Moreover, it was analyzed whether the differentiation molecule triggered the same cell response when being administered only in the basolateral side, or in the basolateral and apical sides of the barrier.

Figure 11 shows that in both concentrations, PMA-free samples present lower TEER values than those supplemented with the differentiation molecule. However, this is not correlated with the presence of the molecule. In order to ensure the exposure to PMA in a compartmentalized manner (only basolateral or both apical and basolateral), the PMA was added on the third last day of culture to samples that did not present leakage so they already had higher TEER values. During the incubation with PMA, the epithelial integrity was not affected since the TEER values did not decrease in any condition. Moreover, no significant difference between PMA applied in the basolateral side or the basolateral and apical sides was observed. These results are also supported by Gjorevski *et al.* who also observed that Caco-2 cells lining a PMA-containing collagen matrix with embedded THP-1, could form a confluent monolayer, and were not affected by the molecule [40].

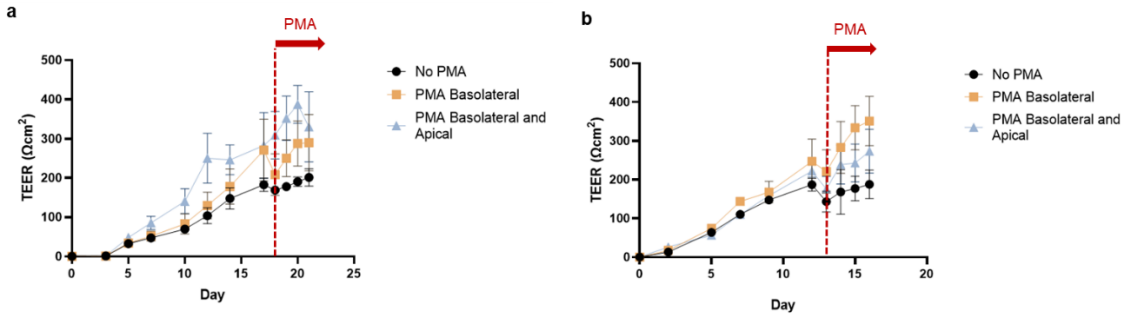

Figure 11. TEER values for samples without PMA, with PMA in the basolateral side, and PMA in the basolateral and apical side at a concentration of 200 nM (a) and 81 nM (b). The values shown are the Mean ± SEM, n=3.

The cell morphology was also evaluated by optical microscopy (Figure 12). The Caco-2 BBe seeded on the surface of the hydrogel formed a confluent and tight monolayer and presented a cobblestone-like morphology for all the conditions (Figure 12 (a, d, g)). As to the cells embedded inside the hydrogel, spherical and elongated NIH-3T3 (Figure 12 (f)) were observed, as well as spherical THP-1 (Figure 12 (b, i)). Interestingly, large globular cells were distinguished in the stromal compartment (Figure 12 (c, e, h)), especially on the PMA treated samples.

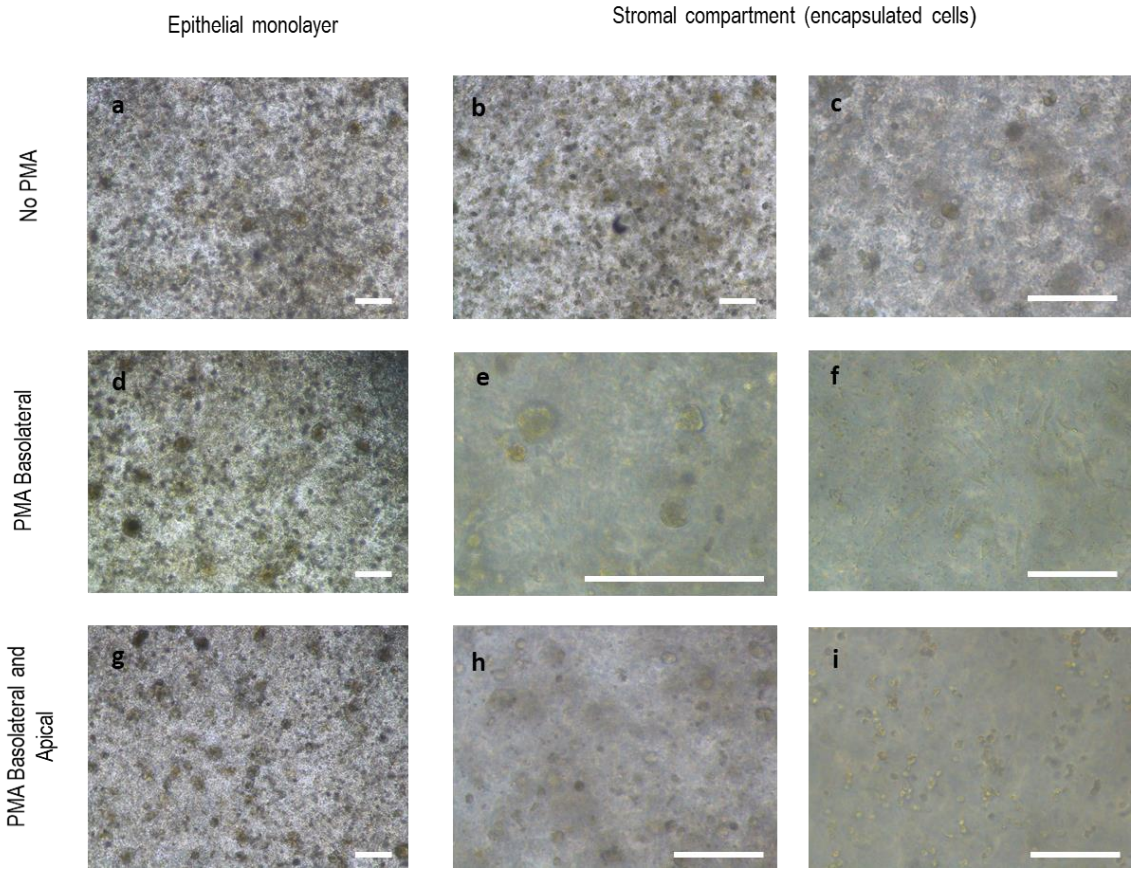

Figure 12. Microscope images of the epithelial monolayer and the stromal compartment, with encapsulated fibroblasts and monocytes (a-c). Samples were exposed to PMA on the basolateral side (d-f), or in the basolateral and apical sides of the barrier (g-i). The epithelial monolayer formed by Caco-2 BBe cells on the surface of the hydrogels can be clearly distinguished (a,d,g). The THP-1 embedded in the hydrogel presented round, single-cell morphology (b, i) whereas encapsulated NIH-3T3 were elongated (f). Large globular cells inside the hydrogel were also observed (c, e, h). Scale bar: 200 µm.

Considering the results, we reaffirm the abovementioned conclusion. Epithelial cells can adhere to the hydrogel and proliferate in the presence of PMA forming a uniform monolayer, and stromal fibroblasts could also spread inside the hydrogel. In the case of the monocytes, the large spherical cells presenting a morphology similar to the macrophages lead us to believe that PMA could induce the differentiation of encapsulated THP-1. To verify this assumption a flow cytometry assay was carried out.

5.4.2. *Hydrogel degradation with Collagenase type II*

Once demonstrated that the PMA did not affect the epithelial monolayer, the differentiation degree of the THP-1 cells inside the hydrogels was evaluated by FACS. First, we needed to develop a protocol to degrade the hydrogel and recover the encapsulated cells without affecting their viability. Hydrogels encapsulating NIH-3T3 at different culture time points were used to optimize the procedure. The hydrogel was digested with collagenase type II and fibroblast retrieval was successfully achieved. The scaffolds were completely digested after 45 min incubated in 300 U/mL filtered collagenase solution. All the hydrogels digested 4 hours, 7 days or 14 days after fabrication were digested at the same rate.

From a single hydrogel, 45% of the total encapsulated cells were recovered after one week of incubation, whereas this percentage increased to 61% after two weeks. The enzymatic digestion did not seem to affect the cell viability as retrieved fibroblasts adhered to the cell culture dish after 15 min of seeding (Figure 13).

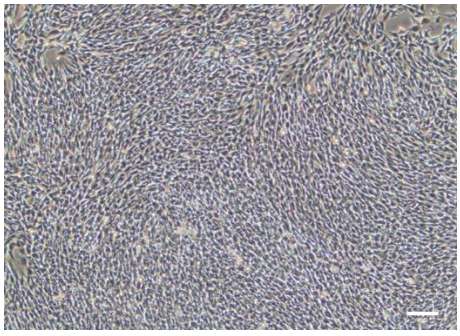

Figure 13. NIH-3T3 recovered from a hydrogel digested 4 hours after printing. Scale bar: 200 µm.

5.4.3. *Flow cytometry direct immunophenotyping*

The differentiation degree of the encapsulated THP-1 cells was assessed by direct immunophenotyping analysis and flow cytometry. CD31 antibody was used to demonstrate the presence of differentiated and non-differentiated THP-1 cells, CD11b antibody to detect differentiated THP-1 (M0) and DAPI for cell viability. To check the specificity of the CD31 and CD11b antibodies, the cell types present in our intestinal mucosal model (Caco-2 BBe, NIH-3T3 and THP-1, differentiated and non-differentiated) were cultivated in standard flasks and trypsinized to get a suspension of around $1x10^6$ cells/mL. Then, the immunophenotyping assay and analysis

by FACS was performed (Figure 14). Isotype controls give the non-specific background signal and determine the fluorescence intensity threshold above which cells are considered positive, so-called gate. As expected, the non-differentiated THP-1 were only positive for CD31, whereas M0 were positive for CD31 and CD11b. Samples with only Caco-2 BBe and NIH-3T3 were negative for both markers (see Appendix B).

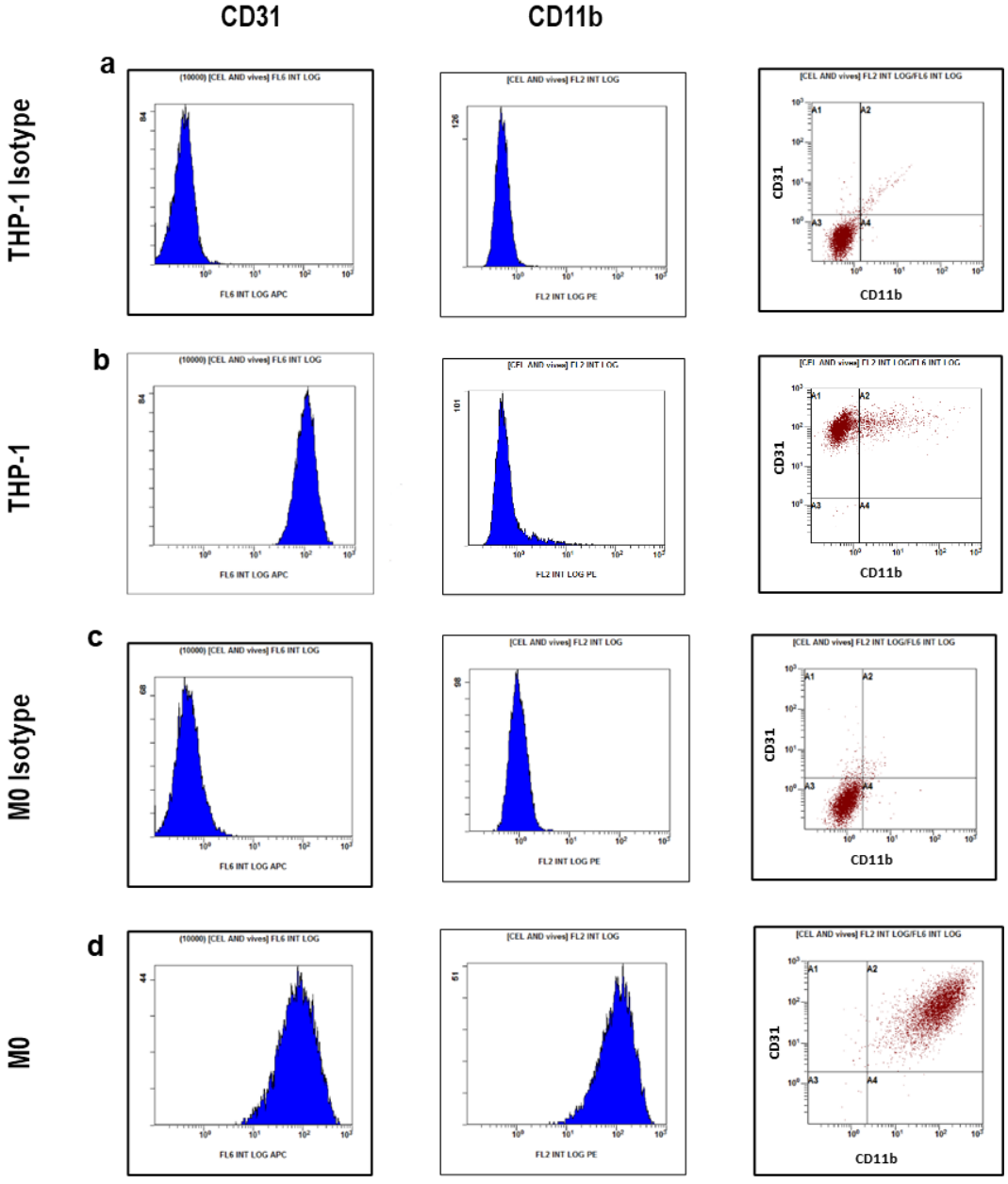

Figure 14. Flow cytometry direct immunophenotyping histograms and dot plots (CD11b vs CD31) of 2D cultures with CD31 and CD11b markers. (a) THP-1 monoculture isotype control. (b) THP-1 monoculture. (c) M0 monoculture isotype control. (d) M0 monoculture.

Then we evaluated if we were able to induce the differentiation of the THP-1 once encapsulated inside the hydrogels. Thus, THP-1 laden hydrogels were printed and exposed to 200 nM PMA for 72 h. As controls, M0 cells that had been differentiated before the hydrogel fabrication were also

encapsulated. Rounded cells were observed in the scaffolds with THP-1 with or without PMA after 2 days of printing, without any noticeable difference between these two conditions (Figure 14 (a, b)). The monocyte-derived macrophages M0 appeared in form of big aggregates (Figure 15 (c)) due to a problem during the hydrogel fabrication. When the bioink was prepared with the cell suspension, the cell pellet was not properly resuspended and clumps of cells were encapsulated inside the hydrogel, instead of a single-cell suspension.

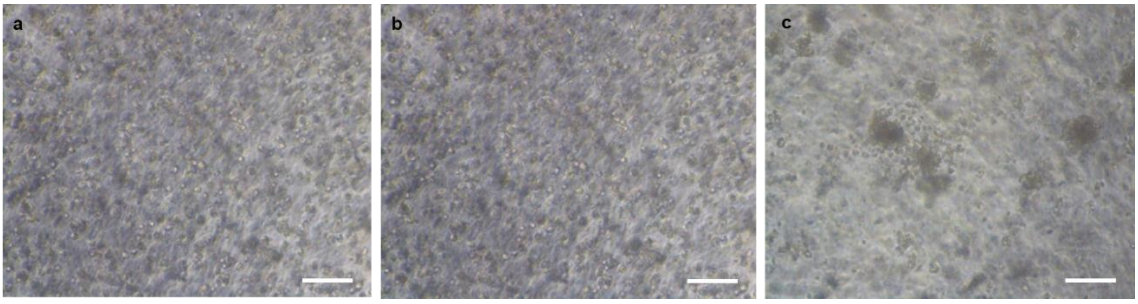

Figure 15. Optical microscope images of cell-laden hydrogels with THP-1 (a), THP-1 exposed to PMA (b) and M0 (c). Scale bar: 100 µm.

After 72 h of PMA treatment, hydrogels were digested, and cells were recovered. The direct immunophenotyping showed that 90% of embedded M0 cells were positive for CD31 and CD11b, meaning that after printing most of the macrophages did not return to the monocytic state (Figure 15). Interestingly, the THP-1 cells had an unexpected behavior. The THP-1 cultivated in 2D were 12.5% positive for CD11b. When these THP-1 cells were encapsulated inside the hydrogels for 3 days, 64% of the cells spontaneously differentiated into CD11b-positive cells. Thereby, it can be deduced that a 3D microenvironment affects cell behavior and promotes cell differentiation. When encapsulated THP-1 were exposed to PMA, this percentage increased to 88%. Thus, PMA can effectively induce monocyte differentiation inside hydrogels.

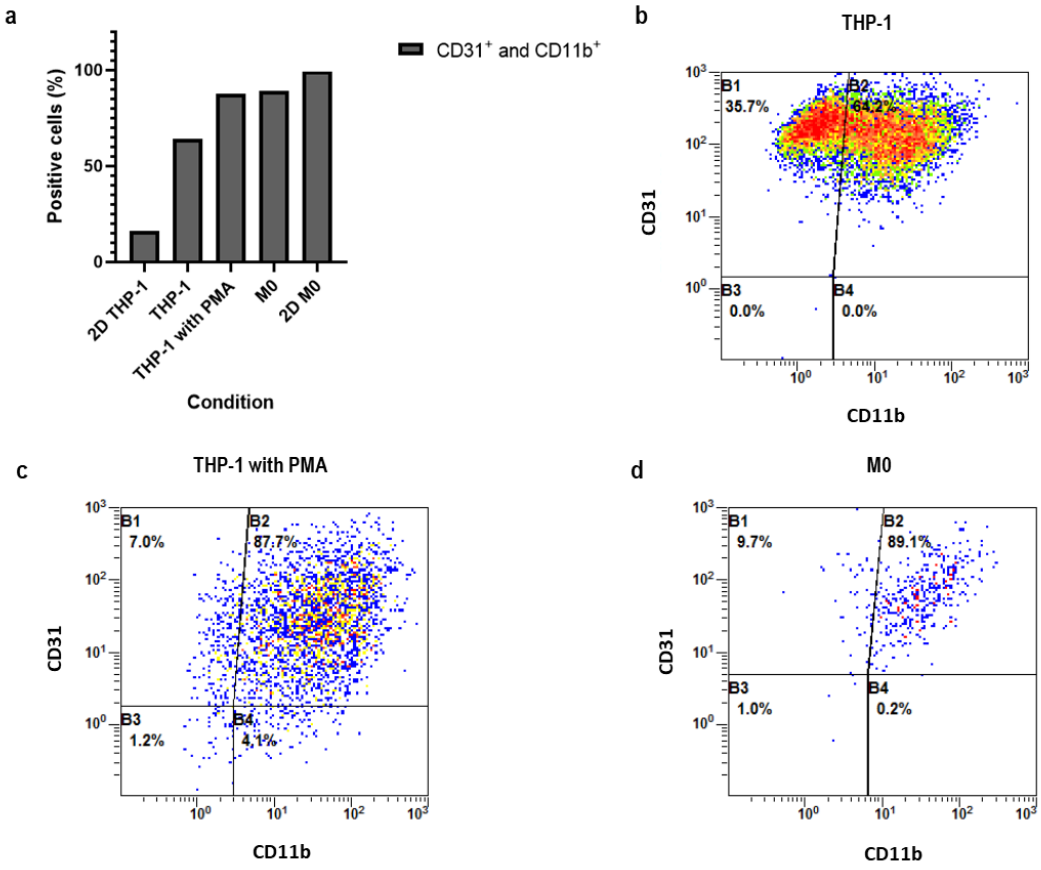

Figure 16. Flow cytometry direct immunophenotyping. (a) Amount of positive cells for markers CD31 and CD11b in 2D and 3D, THP-1 and M0 monocultures. (b) Dot plot (CD31 vs CD11b) of THP-1 encapsulating hydrogels. (c) Dot plot (CD31 vs CD11b) of THP-1 encapsulating hydrogels exposed to PMA. (d) Dot plot (CD31 vs CD11b) of M0 encapsulating hydrogels.

Spontaneous polarization of THP-1 encapsulated in GelMA or PEGDA hydrogels was already reported by Cha *et al* [41]. Monocytes within GelMA scaffolds enlarged and expressed an anti-inflammatory M2-like phenotype whereas when encapsulated in PEGDA hydrogels they differentiated into proinflammatory M1 macrophages. Considering that the main difference of GelMA scaffolds compared to PEGDA is the presence of adhesive motifs, the authors concluded that integrin interactions control the immune response of the monocytes. Similar cell enlargement and differentiation were observed in our monoculture GelMA-PEGDA co-networks, inferring that the architectural environment and material have a critical impact on the behavior of monocytes.

Finally, the behavior of the immune cells was studied in the complete intestinal model, where THP-1 were co-cultured with the NIH-3T3 and Caco-2 BBe cells for 21 days. At day 18, some of the samples were treated with PMA (81 or 200 nM) administered only in the basolateral side or in both apical and basolateral compartments. The differentiation of the THP-1 was studied by FACS (Figure 17). Due to some experimental issues, only the CD11b marker could be used. Without PMA treatment, only 5% of total cells were positive for CD11b. The scaffolds did not only contain THP-1, but also NIH-3T3 and Caco-2 BBe. Thus, the THP-1 cells only accounted for 15% of the total cells.

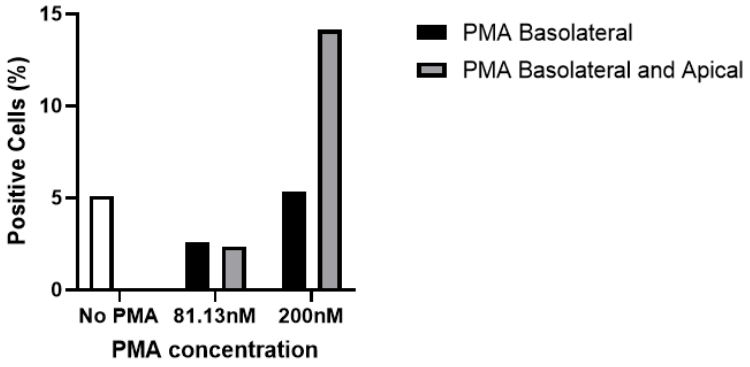

Figure 17. Amount of cells positive for maker CD31 in cell-laden hydrogels cultured in different conditions: without PMA, with PMA on the basolateral side and with PMA on the basolateral and apical side. PMA was administered at a concentration of 81nM or 200nM.

When the THP-1 were exposed to the low PMA concentration, we did not observe an increase in the differentiation rate. However, when cells were incubated with a higher PMA concentration, both apical and basolateral, around 15% of total cells were positive for CD11b. If the proportion of the initial cells was maintained throughout the 3 weeks of culture, this result would mean that almost all the encapsulated cells were differentiated. However, this experiment should be repeated with the CD31 marker to identify the total number of immune cells present in the cell suspension.

5.5. Gut-on-a-chip assembly

Once the cell-laden hydrogels were characterized the gut-on-a-chip model was assembled. Hydrogels encapsulating NIH-3T3 and THP-1 cells were printed with a villi-like architecture, as seen in Figure 18.

First, two cell-laden 3D constructs were incorporated into two single-channel microfluidic chips. After 5 days of perfusion with medium, we did not observe cell migration towards the channels and the cells remained rounded. Some air bubbles appeared as well on the channels of both chips but did not disrupt the hydrogels. Although one of the chips presented leakage and was contaminated with yeast, the other one was used for a Live/Dead™ assay after one week of perfusion. Subsequently, two two-channel microfluidic chips were assembled with cell-encapsulated 3D scaffolds. These chips presented almost no leakage after 5 days of perfusion, however, there was no migration towards the channels. A Live/Dead™ assay was carried out of the two hydrogels after 5 days of perfusion.

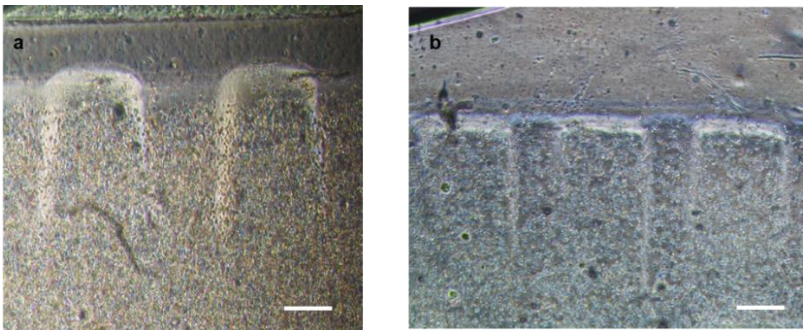

Figure 18. NIH-3T3 and THP-1 encapsulating hydrogels with micropillar structures. (a) Cell-laden hydrogel in a single-channel microfluidic chip, 72 hours after fabrication. (b) Cell-laden hydrogel in a two-channel microfluidic chip, 2 hours after fabrication. Scale bar: 200μm.

To evaluate the cell viability, a Live/Dead™ assay was carried out and the percentage of living cells was calculated in the center and the channel-facing side with the 3D villi structure (Figure 19 (a)). The 3D projections and reconstructions of the confocal images taken from the channel-facing side of the hydrogels are seen in Figure 19 (b,c). All the nuclei are stained with Hoechst reagent, and blue-colored, living cells are depicted in green and dead cells in red. For quantification, cells that presented double staining were considered dead.

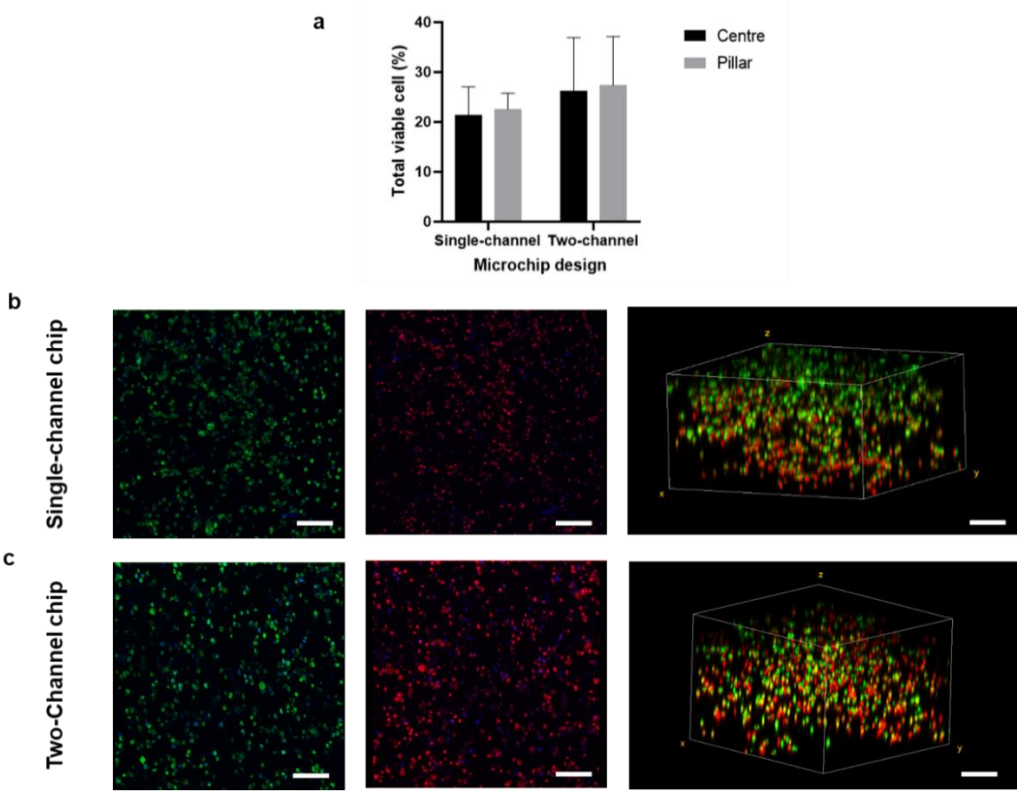

Figure 19. Live/Dead viability/cytotoxicity assay in THP-1 and NIH-3T3 encapsulating hydrogels. The hydrogels were incorporated into single-channel and two-channel microfluidic chip and perfused for 7 and 5 days, respectively. (a) The number of living cells was counted in the area next to the channel and the center of the hydrogel. The values shown are the Mean ± SD, n=2. A minimum of 60 cells were counted from each sample. Maximum intensity projection and 3D reconstruction of confocal images from hydrogels inside single-channel (b) and two-channel (c) chip are also shown. Living cells are stained in green and dead cells in red. Hoechst reagent was used for nuclei staining in blue. Scale bar: 100μm

For both chips, single-channel and two-channels, the cell viability is very low, between 20% and 30%, being slightly higher for the hydrogel in the two-channel chip. Since cell viability in the hydrogels was already confirmed in the flow cytometry tests and other previous studies [21], the PDMS microfluidic system is considered to be responsible for cell toxicity.

One possible explanation may relate to the physical constraints to which the cells are subjected. The holder generates pressure to ensure appropriate sealing and coupling of the two PDMS sheets. Since the hydrogel is in between these two layers, an undesired pressure may be exerted on the scaffold leading to cell death. Studies suggest using PCR adhesive tape for strong bonding between PDMS layers, a simple and low-cost alternative [42].

Another hypothesis would be that the supplemented medium going through the channel cannot reach all the embedded cells. Nevertheless, if this was the cause of cell death, we would expect that the cells near the channels in contact with the medium would have higher viability, but that was not the case. The last possible explanation may be the release of toxic compounds by the PDMS sheets, cured in 3D printed resin molds. The resin, a synthetic organic compound, can still elude soluble substances after polymerization and ultimately alter the PDMS biocompatibility [43].

Almeida Monteuro Melo Ferraz *et al*. demonstrated that solutions incubated in PDMS fabricated using SLA 3D printed resin molds presented leachates [44]. They confirmed that after conditioning the PDMS chip overnight with a medium, removing the eluded substances, the chip could support cell growth. In our work, the molds were only silanized before PDMS curing. Additional steps, such as isopropanol washing reported by previous studies [45], could be implemented in future experiments for PDMS fabrication.

Nonetheless, additional experiments should be carried out to determine if the PDMS fabrication method or the microfluidic chip system need to be modified to ensure cell viability.

6. Execution schedule

6.1. Work Breakdown Structure

The Work Breakdown Structure of the project is depicted in Figure 20.

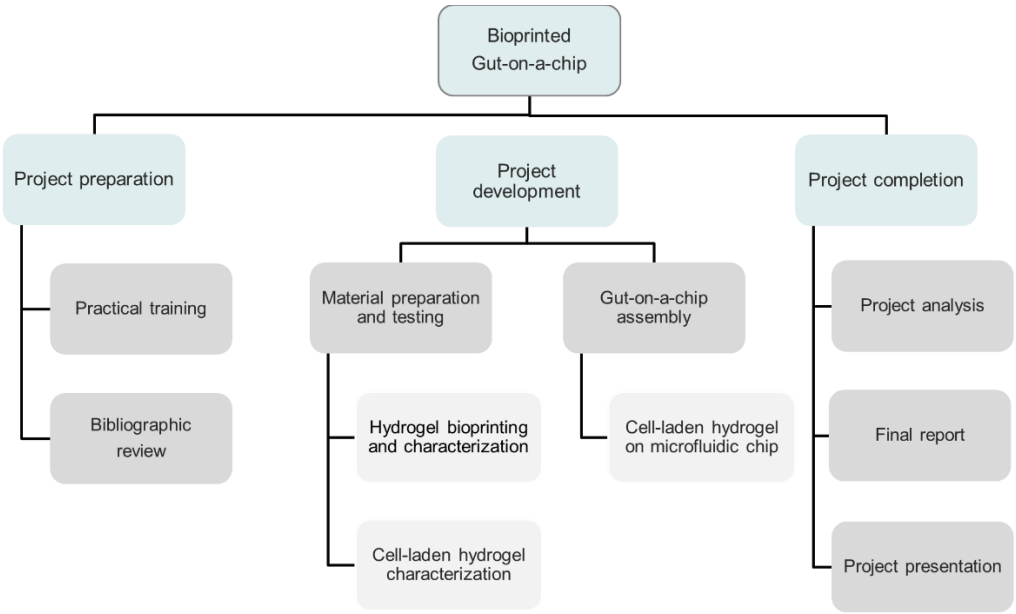

Figure 20. Work Breakdown Structure of the project.

6.2. Task definition

1. Practical training: A training was required before starting the project to use the IBEC facilities and to learn all the basic laboratory tasks - cell passaging and culture maintenance, viability tests, immunofluorescence assays, to name a few.
2. Bibliographic review: To gain insight into biomimetics systems and cell-laden scaffolds, the current state and advancements in the field were reviewed. However, a literature search was carried out throughout the whole project to find new ways of characterizing the cell-laden hydrogels.
3. Hydrogel bioprinting and characterization: The first step in developing the OoC was to prepare the bioink for hydrogel 3D printing. Thus, gelatin must be methacrylized, after which, the bioink with GelMA, PEGDA, LAP and tartrazine solution is prepared, and the hydrogel is bioprinted. Ten, mesh size of the hydrogel is determined. For each experiment, the bioink was freshly prepared.
4. Cell-laden hydrogel characterization: After hydrogel characterization, cell-laden hydrogels were printed. On the one hand, studies of printed hydrogels encapsulating fibroblast and monocytes, together with epithelial cells on the surface were carried out. On the other hand, monocyte behavior inside hydrogels was also assessed.
5. Gut-on-a-chip assembly: Once the components of the OoC were studied and fabricated, the whole gut-on-a-chip, with cell-laden hydrogel, microfluidic chip, holder and hydrogel scaffolds were assembled, and the performance was assessed.

6. Project analysis: After each experiment, the data was processed and analyzed. Yet, a general overview of the outcomes was done after completing all the experiments and before starting the final report.
7. Final Report: This is the final step of the project that consisted of gathering all the information regarding OoC, the experiments, and the results.
8. Project presentation: After report delivery, the project will be presented and discussed in front of a jury.

6.3. PERT-CPM

In Table 1 the tasks involved in the project, order of execution, and duration are shown.

Task	Activity	Previous activities	Next activities	Duration (Weeks)
A	Practical training	-	C, D, E	9
B	Bibliographic review	-	D, G	30
C	Hydrogel bioprinting and characterization	A	D, E	20
D	Cell-laden hydrogel characterization	B, C	E	10
E	Gut-on-a-chip assembly	C, D	F	3
F	Project analysis	E	G	2
G	Final report	B,F	H	5
H	Project presentation	G	-	1

Table 1. Project task sequence and duration (in weeks).

From the task planning the PERT-CPM charts were created (Figure 21).

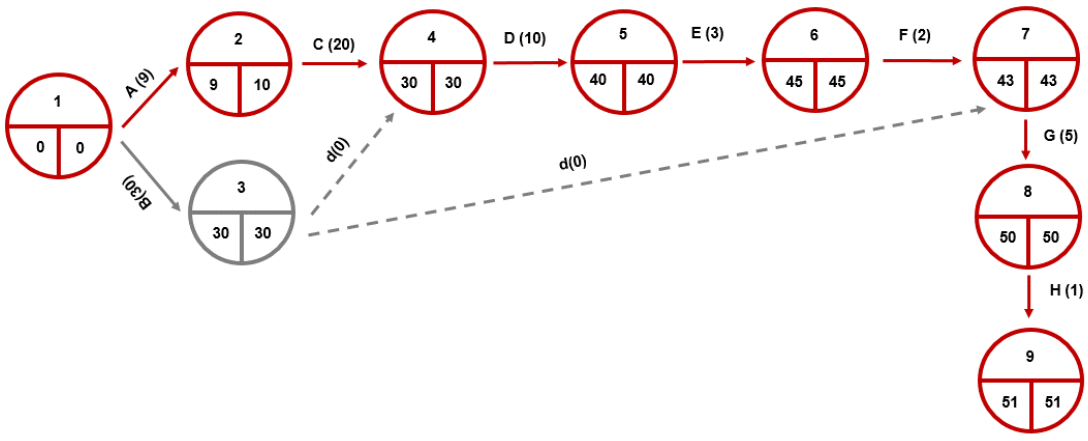

Figure 21. PERT diagram of the project with the critical path indicated by the red-colored circles.

6.4. GANTT Chart

The detailed timeline of the tasks was represented with a GANTT chart (Figure 22).

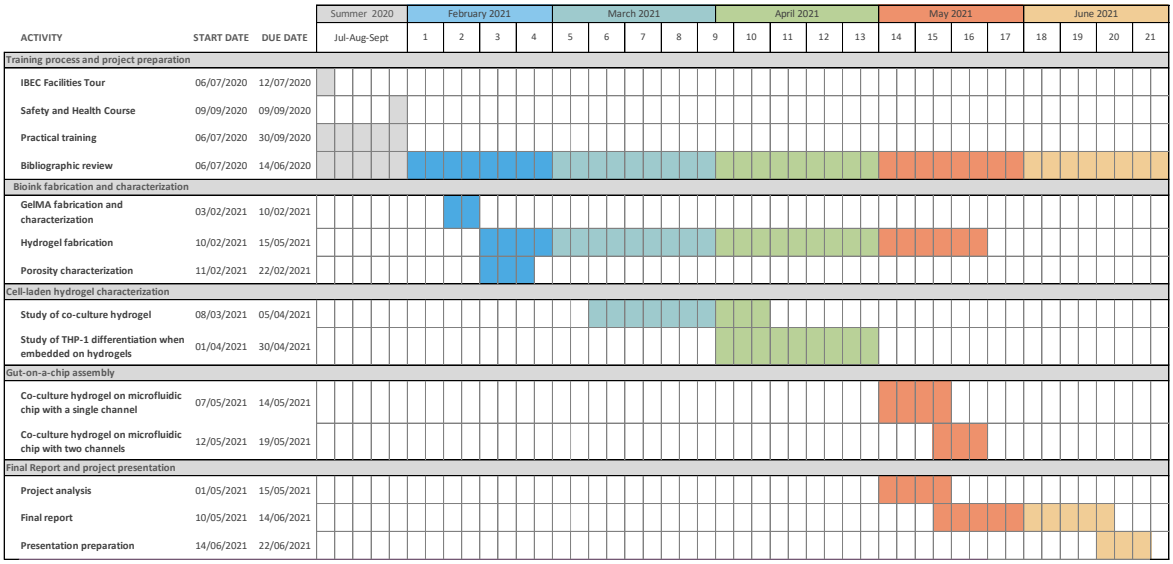

Figure 22. Detailed GANTT Chart of the activities carried throughout the project.

7. Technical feasibility

Table 2 shows the strength, weaknesses, opportunities, and threats (SWOT) analysis of the project.

Strengths	Weaknesses
- Mimics the in-vivo 3D architecture. - Co-cultured hydrogels that support cell-cell interaction. - Device with immunocompetent features for inflammatory analysis. - Use of simple and reproducible bioprinting and microfluidics technology. - High-resolution and control of the microenvironment architecture. - Real-time and on-chip analysis.	- Low cell viability in hydrogels inside the microfluidic chip. - Leakage and air bubble formation inside the microfluidic chip. - Require controlled temperature and humidity conditions for bioprinting. - Lack of peristaltic motion.
Opportunities	**Threats**
- Increase demand of OoC. - Increase areas of application. - Automated bioprinting of cell-laden hydrogels. - Integration of sensors.	- No current legislation or validation method. - End-users, specifically the pharmaceutical industry, are in a highly regulated environment to predict drug responses and toxicological outcomes.

Table 2. SWOT analysis of the project.

8. Economic viability

The materials and equipment used in the project were provided by the Biomimetic System for Cell Engineering research group and by the IBEC Core facilities. These last ones had an additional cost specified in Table 3.

Equipment	Hours	Price rate (€/h)
Oven	6	4.44
ProCleaner™	3	2
3D Printer Solus CleanRoom	25	16.52
Confocal Microscopy	12	28
M200 PRO Multimode Microplate Reader	4	20
Gallios Research Flow cytometer	10	28

Table 3. Hours of use and price rates of the equipment provided by Core Facilities, IBEC.

The reagents, materials and software used with their correspondent cost are shown in Table 4.

Resource	Units	Cost (€)
Reagents		
Dulbecco's Modified Eagle Medium (DMEM)	500 mL	25.8
Roswell Park Memorial Institute (RPMI)-1640 medium	500 mL	31.44
Fetal Bovine Serum (FBS)	125 mL	175
Trypsin-EDTA	60 mL	10.5
Penicillin/Streptomycin (Pen/Strep)	20 mL	10.5
Sodium pyruvate	5 mL	0.1
4-(2-hydroxyethyl)-1-piperazineethanesulfonic acid	5 mL	7.2
β-mercaptoethanol	500 μL	0.5
Phorbol 12-myristate 13-acetate (PMA)	100 ng	1
Accutase®	10 mL	5.5
Phosphate Buffered Saline Solution	1 L	90.5
Gelatin porcine skin type A	10 g	2.75
Methacrytic anhydride	5 mL	0.72
2,4,6 – Trinitrobenzene sulfonic acid (TNSBA)	20 μL	0.5
Sodium dodecyl sulfate (SDS)	5 mL	0.1
Sodium bicarbonate solution ($NaHCO_3$)	1 mL	0.1
Hydrochloric acid (HCl)	500 μL	1.5
Lithium arylphosphanate	40 mg	4
Poly(ethylene glycol) diacrylate	300 mg	64.5
Tartrazine	2.5 mg	1
Hank's Balanced Salt Solution (HBSS)	10 mL	0.5
3-(Trimethoxysilyl) propyl methacrylate	0.2 mL	0.1
Acetic acid	0.3 mL	4
FITC-dextrans	8.8 mg	11.2
70 kDa Rhodamine-dextran (FD70)	2.2 mg	30.8
Normocin	600 μL	7.6
Collagenase type II	5 mg	2
Sodium azide	250 mg	0.1
CD31 Antibody and Isotype	75 μL	57.3
CD11b Antibody and Isotype	150 μL	114.6

Live/Dead™ viability/cytotoxicity assay kit	9 μL	150
Hoechst	6 μL	0.1
Polydimethylsiloxane (PDMS) pre-polymer elastomer and curing agent	1 kg	173
Materials		
Dialysis membranes	20	30.8
Labware	N/A	600
Labcoat	1	25
Laboratory notebook	1	15
Softwares		
FreeCAD	N/A	0
Fiji-ImageJ	N/A	0
Microsoft 365	N/A	0
Graphic Tools	N/A	0
	Total cost	1651.31

Table 4. Reagents, materials, and software used throughout the project.

Considering the price of the equipment, the reagents and products used, and the supervision and tutoring from an experienced researcher (25€/h) the total project expenditure was of around 5000€.

9. Regulation and legal aspects.

Given the infancy of this technology, no specific regulations or standards have been defined. Consequently, a regulatory framework and body that facilitate the validation process of organ-on-a-chip models for its future application are needed. With this objective in mind, the EU initiated the ORCHID project in 2017. The project, coordinated by Leiden University Medical Center and the Dutch Organ-on-Chip consortium hDMT, had the goal of assessing the current technology status, presenting guidance for regulation and standardization, identifying a roadmap for technology adoption, and raising awareness. After the project's termination in 2019, the European Organ-on-Chip Society (EUROoCS) was born. This consortium has taken the lead in building a network that includes regulatory bodies, end-users and developers, supporting OoC development and creating a roadmap and guidelines for OoC implementation. The defined roadmap consists of six steps: application, specification, qualification, standardization, production and upscaling, and adoption [46].

In this context, the JRC's European Union Reference Laboratory for alternatives to animal testing (EURL ECVAM) also plays a key role. Their goal is to ensure the EU member states' compliance with the 3R's principle (replacement, reduction and refinement) defined in the Directive 2010/63/EU to minimize animal testing for scientific and educational purposes. The European body is

responsible for validating the alternatives, in which the OoC would be included, with the help of an independent Scientific Advisory Committee (ESAC). Moreover, they are currently collaborating with the EUROoCS in the implementation of quality control assays carried out by testing centres to evaluate the performance of the *in vitro* models [47].

Despite the lack of availability of specific regulations, some existing international quality standards can be applied to OoCs. For instance, the Medical Devices-Quality Management System (ISO 13485:2016) sets the requirements to ensure the robustness, reproducibility, and reliability of the models.

Finally, as we are working with biological agents we should adhere to the following guidelines: *Directive 2000/54/EC of the European Parliament and of the Council of 18 September 2000 on the protection of workers from risks related to exposure to biological agents at work.*

10. Conclusion and future directions.

OoC is an emerging technology that has caught the attention of the pharmaceutical industry, and potentially the healthcare sector for personalized medicine. In only ten years' time new companies and research groups have been able to find new efficient, effective, and cost-saving methods for *in vitro* drug screening and human physiology studies. However, currently available OoCs lack complex tissue features limiting the translational capabilities of the devices to clinical outcomes. This aspect is crucial in organs such as the gut, which have a very characteristic architecture that must be emulated in order to get a reliable model. For fabricating these ECM-like constructs, 3D bioprinting techniques are being explored due to its simplicity, reproducibility and precision.

Therefore, in the present project, we attempted to develop a gut-on-a-chip device that mimicked the small intestinal mucosa combining SLA 3D bioprinting with microfluidic technology. We aimed to fabricate a 3D bioprinted cell-encapsulating hydrogel with villus-crypt architecture that supported epithelial monolayer formation on top, which would be later incorporated into a PDMS microfluidic chip. The 3D constructs are fabricated with the object of replicating the two layers in the intestinal mucosa; the lamina propria and the intestinal barrier.

The stromal compartment was successfully reproduced by GelMA-PEGDA bioprinted hydrogels with embedded fibroblasts and monocytes. The scaffolds were printed with the SLA technique and provided a suitable environment for NIH-3T3 and THP-1 adhesion and proliferation, as well as subsequent epithelial monolayer formation. This last process was proved to be accelerated by the secretion of ECM by encapsulated NIH-3T3.

Furthermore, the incorporation of immune cells into the model was of great interest due to the key role resident macrophages play in intestinal homeostasis. In this study, hydrogel-embedded THP-

1 differentiation into macrophages was accomplished with the diffusion of PMA through the pores of the hydrogels. Interestingly, it was observed that the 3D microenvironment alone induced the spontaneous differentiation of monocytes into the phagocytic cells.

The ability of PMA induced differentiation in complete 3D intestinal models, this is, NIH-3T3 and THP-1 encapsulating hydrogels with Caco-2 BBe seeded on top, was also analyzed. It was demonstrated that PMA did not affect the barrier integrity. Even though some cells presented macrophage-like morphology in the PMA exposed models, further experiments are needed to verify and quantify monocyte differentiation.

Lastly, SLA bioprinting allowed for the fabrication of rectangular cell-laden hydrogels with crypt-villus architecture on one side. However, the incorporation of this hydrogel inside the microfluidic system resulted in cell death. The cause is yet to be determined, although possible explanations are excess compression or the release of leachates by the cured PDMS in 3D printed resin molds. Thus, future experiments need to focus on and the improvement of the PDMS chip and holder system to ensure cell viability. Once this is guaranteed, the next step would be to seed the side-channel facing surface of the hydrogel with Caco-2 BBe to model the epithelial barrier, by perfusion of epithelial cell suspension through the channel.

Hereafter, the complexity and functionality of the biomimetic systems can be increased with the incorporation of biomechanical or chemical cues as well as the integration of biosensors for *in situ* monitoring of functional parameters. With regards to the fabrication process, given the importance of rapid and precise fabrication in the OoC market, the current bioprinting setup should be optimized and automated, as the current configuration is optimized for single scaffold bioprinting. Lastly, the robustness and predictiveness of the model should be assessed, to guarantee stable experimental conditions when used in drug screening and toxicity tests.

While there is still a lot of room for improvement, this biomimetic gut-on-a-chip device might potentially be used to study intestinal physiology and disease mechanisms, as it replicates many of the relevant features of the native human gut.

11. Bibliography

[1] S. N. Bhatia and D. E. Ingber, "Microfluidic organs-on-chips," *Nature Biotechnology*, vol. 32, no. 8. Nature Publishing Group, pp. 760–772, 2014, doi: 10.1038/nbt.2989.

[2] A. M. Ghaemmaghami, M. J. Hancock, H. Harrington, H. Kaji, and A. Khademhosseini, "Biomimetic tissues on a chip for drug discovery," *Drug Discovery Today*, vol. 17, no. 3–4. NIH Public Access, pp. 173–181, Feb. 2012, doi: 10.1016/j.drudis.2011.10.029.

[3] J. E. Sosa-Hernández *et al.*, "Organs-on-a-chip module: A review from the development and applications perspective," *Micromachines*, vol. 9, no. 10. MDPI AG, Oct. 22, 2018, doi: 10.3390/mi9100536.

[4] E. Salvo-Romero, C. Alonso-Cotoner, C. Pardo-Camacho, M. Casado-Bedmar, and M. Vicario, “The intestinal barrier function and its involvement in digestive disease,” 2015. Accessed: Jun. 07, 2021. [Online].

[5] M. M. Maxime, N. E. Brown, H. M. Poling, and H. A. Michael, “In vivo model of small intestine,” in *Methods in Molecular Biology*, vol. 1597, Humana Press Inc., 2017, pp. 229–245.

[6] F. T. Bosman, A. de Bruine, C. Flohil, A. van der Wurff, J. ten Kate, and W. W. M. Dinjens, “Epithelia-stromal interactions in colon cancer,” *International Journal of Developmental Biology*, vol. 37, no. 1. UPV/EHU Press, pp. 203–211, Feb. 01, 1993, doi: 10.1387/ijdb.8507562.

[7] G. M. Whitesides, “The origins and the future of microfluidics,” *Nature*, vol. 442, no. 7101. pp. 368–373, Jul. 27, 2006, doi: 10.1038/nature05058.

[8] N. Y. Lee, “Recent progress in lab-on-a-chip technology and its potential application to clinical diagnoses,” *International Neurourology Journal*, vol. 17, no. 1, pp. 2–10, Mar. 2013, doi: 10.5213/inj.2013.17.1.2.

[9] Q. Wu *et al.*, “Organ-on-a-chip: Recent breakthroughs and future prospects,” *BioMedical Engineering Online*, vol. 19, no. 1. BioMed Central Ltd., Feb. 12, 2020, doi: 10.1186/s12938-020-0752-0.

[10] H. J. Kim, D. Huh, G. Hamilton, and D. E. Ingber, “Human gut-on-a-chip inhabited by microbial flora that experiences intestinal peristalsis-like motions and flow,” *Lab on a Chip*, vol. 12, no. 12, pp. 2165–2174, Jun. 2012, doi: 10.1039/c2lc40074j.

[11] M. Nikolaev *et al.*, “Homeostatic mini-intestines through scaffold-guided organoid morphogenesis,” *Nature*, vol. 585, no. 7826, pp. 574–578, Sep. 2020, doi: 10.1038/s41586-020-2724-8.

[12] T. Nguyen, S. H. Jung, M. S. Lee, T. E. Park, S. K. Ahn, and J. H. Kang, “Robust chemical bonding of PMMA microfluidic devices to porous PETE membranes for reliable cytotoxicity testing of drugs,” *Lab on a Chip*, vol. 19, no. 21, pp. 3706–3713, Nov. 2019, doi: 10.1039/c9lc00338j.

[13] P. G. Miller and M. L. Shuler, “Design and demonstration of a pumpless 14 compartment microphysiological system,” *Biotechnology and Bioengineering*, vol. 113, no. 10, pp. 2213–2227, Oct. 2016, doi: 10.1002/bit.25989.

[14] J. R. Puryear, J. K. Yoon, and Y. T. Kim, “Advanced fabrication techniques of microengineered physiological systems,” *Micromachines*, vol. 11, no. 8. MDPI AG, Aug. 01, 2020, doi: 10.3390/MI11080730.

[15] H. Geckil, F. Xu, X. Zhang, S. Moon, and U. Demirci, “Engineering hydrogels as extracellular matrix mimics,” *Nanomedicine*, vol. 5, no. 3. NIH Public Access, pp. 469–484, Apr. 2010, doi: 10.2217/nnm.10.12.

[16] Ž. Kačarević *et al.*, "An Introduction to 3D Bioprinting: Possibilities, Challenges and Future Aspects," *Materials*, vol. 11, no. 11, p. 2199, Nov. 2018, doi: 10.3390/ma11112199.

[17] A. Bein *et al.*, "Microfluidic Organ-on-a-Chip Models of Human Intestine," *CMGH*, vol. 5, no. 4. Elsevier Inc, pp. 659–668, Jan. 01, 2018, doi: 10.1016/j.jcmgh.2017.12.010.

[18] D. Gao, H. Liu, J. M. Lin, Y. Wang, and Y. Jiang, "Characterization of drug permeability in Caco-2 monolayers by mass spectrometry on a membrane-based microfluidic device," *Lab on a Chip*, vol. 13, no. 5, pp. 978–985, Mar. 2013, doi: 10.1039/c2lc41215b.

[19] G. Altay, S. Tosi, M. García-Díaz, and E. Martínez, "Imaging the Cell Morphological Response to 3D Topography and Curvature in Engineered Intestinal Tissues," *Frontiers in Bioengineering and Biotechnology*, vol. 8, Apr. 2020, doi: 10.3389/fbioe.2020.00294.

[20] K. Y. Shim, D. Lee, J. Han, N. T. Nguyen, S. Park, and J. H. Sung, "Microfluidic gut-on-a-chip with three-dimensional villi structure," *Biomedical Microdevices*, vol. 19, no. 2, pp. 1–10, Jun. 2017, doi: 10.1007/s10544-017-0179-y.

[21] A. Vila *et al.*, "Hydrogel co-networks of gelatine methacrylate and poly(ethylene glycol) diacrylate sustain 3D functional in vitro models of intestinal mucosa," *Biofabrication*, vol. 12, no. 2, p. 025008, Feb. 2020, doi: 10.1088/1758-5090/ab5f50.

[22] A. V. Giraut, "Hydrogel co-networks of gelatin methacryloyl and poly(ethylene glycol)diacrylate sustain 3D functional in vitro models of intestinal mucosa," Universitat de Barcelona, Dec. 2020. Accessed: Jun. 10, 2021. [Online]. Available: http://diposit.ub.edu/dspace/handle/2445/174226.

[23] W. L. A. Liew and Y. Zhang, "Laser-based fabrication of 3D hydrogel constructs using bessel beams," *Bioprinting*, vol. 9, pp. 44–51, Mar. 2018, doi: 10.1016/j.bprint.2018.02.004.

[24] D. Huh, B. D. Matthews, A. Mammoto, M. Montoya-Zavala, H. Yuan Hsin, and D. E. Ingber, "Reconstituting organ-level lung functions on a chip," *Science*, vol. 328, no. 5986, pp. 1662–1668, Jun. 2010, doi: 10.1126/science.1188302.

[25] M. Kasendra *et al.*, "Development of a primary human Small Intestine-on-a-Chip using biopsy-derived organoids," *Scientific Reports*, vol. 8, no. 1, p. 2871, Dec. 2018, doi: 10.1038/s41598-018-21201-7.

[26] "Microfluidics Market Size | Industry Report, 2021-2028." https://www.grandviewresearch.com/industry-analysis/microfluidics-market (accessed Jun. 07, 2021).

[27] N. Azizipour, R. Avazpour, D. H. Rosenzweig, M. Sawan, and A. Ajji, "Evolution of biochip technology: A review from lab-on-a-chip to organ-on-a-chip," *Micromachines*, vol. 11, no. 6, pp. 1–15, Jun. 2020, doi: 10.3390/mi11060599.

[28] P. Thayer, H. Martinez, and E. Gatenholm, “Chapter 1 History and Trends of 3D Bioprinting,” pp. 3–18, 2020, doi: 10.1007/978-1-0716-0520-2_1.

[29] “Global 3D Bioprinting Market Size & Trends Report 2021-2028.” https://www.grandviewresearch.com/industry-analysis/3d-bioprinting-market (accessed Jun. 07, 2021).

[30] A. I. van den Bulcke, B. Bogdanov, N. de Rooze, E. H. Schacht, M. Cornelissen, and H. Berghmans, “Structural and rheological properties of methacrylamide modified gelatin hydrogels,” *Biomacromolecules*, vol. 1, no. 1, pp. 31–38, 2000, doi: 10.1021/bm990017d.

[31] A. F. S. A. Habeeb, “Determination of free amino groups in proteins by trinitrobenzenesulfonic acid,” *Analytical Biochemistry*, vol. 14, no. 3, pp. 328–336, Mar. 1966, doi: 10.1016/0003-2697(66)90275-2.

[32] A. G. Castaño, M. García-Díaz, N. Torras, G. Altay, J. Comelles, and E. Martínez, “Dynamic photopolymerization produces complex microstructures on hydrogels in a moldless approach to generate a 3D intestinal tissue model,” *Biofabrication*, vol. 11, no. 2, p. 25007, Feb. 2019, doi: 10.1088/1758-5090/ab0478.

[33] C. M. Murphy and F. J. O, “Cell Adhesion & Migration Understanding the effect of mean pore size on cell activity in collagen-glycosaminoglycan scaffolds,” 2010, doi: 10.4161/cam.4.3.11747.

[34] K. Engberg and C. W. Frank, “Protein diffusion in photopolymerized poly(ethylene glycol) hydrogel networks,” *Biomedical Materials*, vol. 6, no. 5, 2011, doi: 10.1088/1748-6041/6/5/055006.

[35] K. A. Wodzanowski, A. M. Kloxin, and C. L. Grimes, “Multiscale Invasion Assay for Probing Macrophage Response to Bacteria,” *bioRxiv*, p. 2020.11.16.385617, Nov. 2020, doi: 10.1101/2020.11.16.385617.

[36] S. A. Bencherif, A. Srinivasan, F. Horkay, J. O. Hollinger, K. Matyjaszewski, and N. R. Washburn, “Influence of the degree of methacrylation on hyaluronic acid hydrogels properties,” 2008, doi: 10.1016/j.biomaterials.2007.11.047.

[37] J. W. Nichol, S. T. Koshy, H. Bae, C. M. Hwang, S. Yamanlar, and A. Khademhosseini, “Cell-laden microengineered gelatin methacrylate hydrogels,” *Biomaterials*, vol. 31, no. 21, pp. 5536–5544, Jul. 2010, doi: 10.1016/j.biomaterials.2010.03.064.

[38] S. M. Lien, L. Y. Ko, and T. J. Huang, “Effect of pore size on ECM secretion and cell growth in gelatin scaffold for articular cartilage tissue engineering,” *Acta Biomaterialia*, vol. 5, no. 2, pp. 670–679, Feb. 2009, doi: 10.1016/j.actbio.2008.09.020.

[39] S. Wang, Q. Ye, X. Zeng, and S. Qiao, “Functions of macrophages in the maintenance of intestinal homeostasis,” *Journal of Immunology Research*, vol. 2019. Hindawi Limited, 2019, doi: 10.1155/2019/1512969.

[40] N. Gjorevski *et al.*, "Neutrophilic infiltration in organ-on-a-chip model of tissue inflammation," *Lab on a Chip*, vol. 20, no. 18, pp. 3365–3374, Sep. 2020, doi: 10.1039/d0lc00417k.

[41] B. H. Cha *et al.*, "Integrin-Mediated Interactions Control Macrophage Polarization in 3D Hydrogels," *Advanced Healthcare Materials*, vol. 6, no. 21, p. 1700289, Nov. 2017, doi: 10.1002/adhm.201700289.

[42] M. Serra, I. Pereiro, A. Yamada, J. L. Viovy, S. Descroix, and D. Ferraro, "A simple and low-cost chip bonding solution for high pressure, high temperature and biological applications," *Lab on a Chip*, vol. 17, no. 4, pp. 629–634, Feb. 2017, doi: 10.1039/c6lc01319h.

[43] M. Goldberg, "In vitro and in vivo studies on the toxicity of dental resin components: A review," *Clinical Oral Investigations*, vol. 12, no. 1. Springer, pp. 1–8, Mar. 27, 2008, doi: 10.1007/s00784-007-0162-8.

[44] M. de Almeida Monteiro Melo Ferraz, J. B. Nagashima, B. Venzac, S. le Gac, and N. Songsasen, "3D printed mold leachates in PDMS microfluidic devices," *Scientific Reports*, vol. 10, no. 1, pp. 1–9, Dec. 2020, doi: 10.1038/s41598-020-57816-y.

[45] J. Shrestha *et al.*, "A rapidly prototyped lung-on-a-chip model using 3D-printed molds," *Organs-on-a-Chip*, vol. 1, p. 100001, Dec. 2019, doi: 10.1016/j.ooc.2020.100001.

[46] M. Mastrangeli *et al.*, "Organ-on-Chip In Development ORCHID Final Report." Accessed: Jun. 10, 2021. [Online].

[47] "JRC Publications Repository - Non-animal Methods in Science and Regulation." https://publications.jrc.ec.europa.eu/repository/handle/JRC123531 (accessed Jun. 10, 2021).

[48] C. J. Lee, J. A. Vroom, H. A. Fishman, and S. F. Bent, "Determination of human lens capsule permeability and its feasibility as a replacement for Bruch's membrane," *Biomaterials*, vol. 27, no. 8, pp. 1670–1678, Mar. 2006, doi: 10.1016/j.biomaterials.2005.09.008.

12. Appendix

Appendix A

The diffusion coefficient of each dextran in the hydrogels was also calculated through the formulas extracted from Engberg *et al*.

$$-\ln\left(1-\frac{C_n(t)}{\frac{N}{V}}\right)=\frac{D_{gel}}{h}\left(\frac{t}{\tau}\right) \qquad \textit{Eq. 4}$$

$$V = V_d + Ah + V_r \qquad \textit{Eq. 5}$$

$$\tau = \frac{\left(V_d + \frac{Ah}{2}\right)\left(V_r + \frac{Ah}{2}\right)}{AV} \qquad \textit{Eq. 6}$$

Where *h* is the thickness of the hydrogel and *N* the initial mass of the solute. Finally, the diffusion coefficient of the dextrans in the hydrogels can be compared to the diffusion in water, calculated with the Stokes-Einstein equation:

$$D_0 = \frac{K_B T}{6hpr} \qquad \textit{Eq. 7}$$

Considering that the hydrogels were printed on top of PET membranes the diffusion coefficient of the dextrans through the membranes was also assessed. The diffusion coefficient of the hydrogels was then calculated, considering a dual membrane (hydrogel and PET membrane) configuration. To do so, the equations extracted from C.J Lee *et al*.[48] were used:

$$-\ln\left(1 - \frac{C_n(t)}{\frac{N}{V}}\right) = \frac{1}{\frac{h_{gel}}{D_{gel}} + \frac{h_{PET}}{D_{PET}}} * \frac{t}{\tau} \qquad \textit{Eq. 8}$$

$$V = V_d + Ah + V_r \qquad \textit{Eq. 9}$$

$$\tau = \frac{\left(V_d + \frac{A * \left(h_{PET} + h_{gel}\right)}{2}\right) * \left(V_r + \frac{A * \left(h_{PET} + h_{gel}\right)}{2}\right)}{AV} \qquad \textit{Eq. 10}$$

The diffusion coefficient for dextrans of 4kDa, 70 kDa, 150 kD, 500 kDa and 2000 kDa in the hydrogels, subtracting the effect of the membrane, are shown in Figure 23 (a). The ratio of diffusion through hydrogel and diffusion through water has been also calculated (Figure 23 (b)).

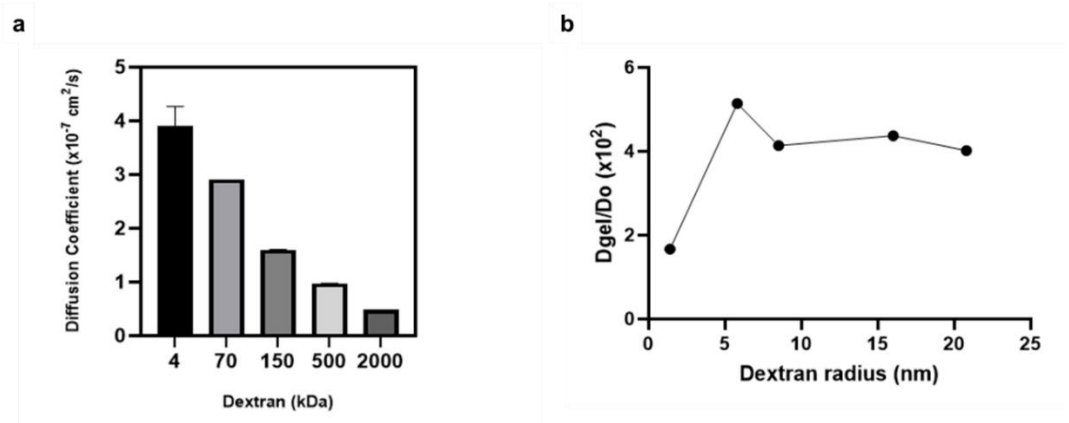

Figure 23. Hydrogel pore size characterizatio. (a) Diffusion coefficient in the hydrogel of the dextrans with a molecular weight of 4kDa, 70kDa, 150kDa, 500kDa and 2000kDa. The values shown are mean ± SD, n>2. (b) Ratio between the diffusion coefficient in the hydrogel and water of the different dextrans. The values shown are mean, n>2.

Appendix B

A direct immunophenotyping analysis and flow cytometry assay with marker CD11b (Figure 24) and CD31 (Figure 25) in cultures of Caco-2 BBe and NIH-3T3 was also carried out to verify the specificity of these markers for THP-1 and M0. Isotype and autofluorescence controls were included to determine the non-specific background signal. Assays with the CD11b marker were analyzed with the FACSAria™ III Cell sorter (BD, Biosciences), whereas those with CD31 marker were analyzed with Gallios Research Flow cytometry (Beckman Coulter).

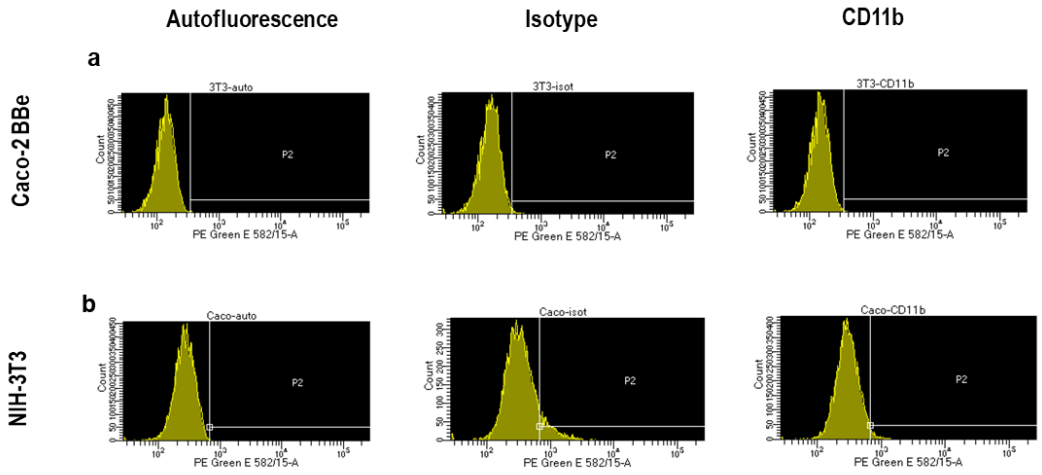

Figure 24. Direct immunophenotyping assay and analysis by FACS with marker CD11b of Caco-2 BBe (a) and NIH-3T3 (b) 2D cultures, including autofluorescence and isotype controls.

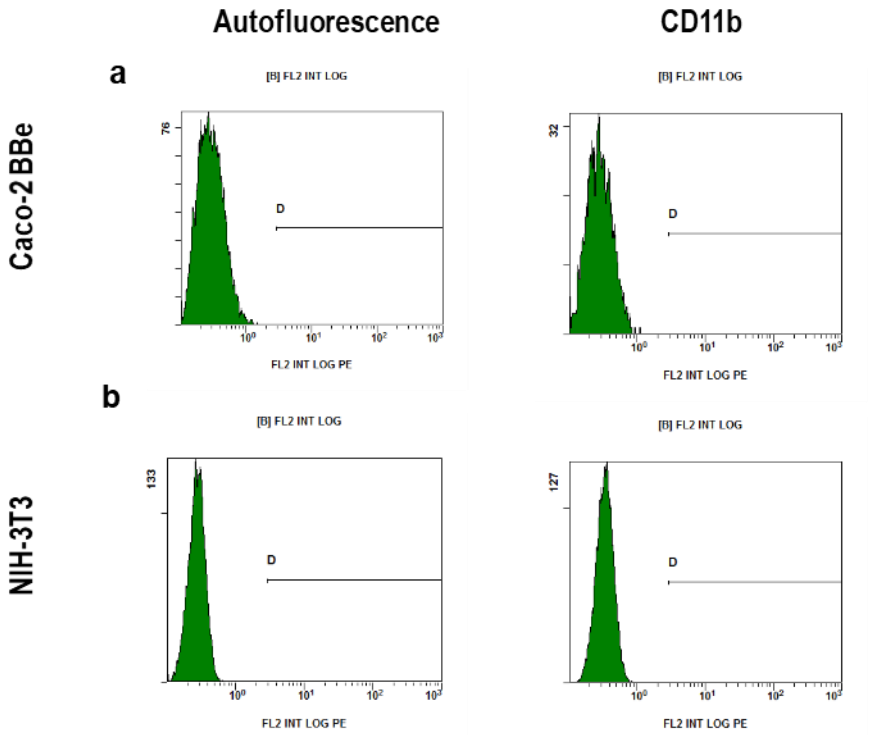

Figure 25. Direct immunophenotyping assay and analysis by FACS with marker CD31 of Caco-2 BBe (a) and NIH-3T3 (b) 2D cultures, including isotype controls.